1   **Expanding seawater carbon dioxide and methane measuring capabilities with a Seaglider**

2

3   Claudine Hauri[1*], Brita Irving[1], Dan Hayes[2], Ehsan Abdi[3,4], Jöran Kemme[5], Nadja Kinski[5], and

4   Andrew M. P. McDonnell[6,7]

5

6   [1]International Arctic Research Center, University of Alaska Fairbanks, Fairbanks, AK 99775,

7   USA

8   [2]Advanced Offshore Operations, Inc., Houston, TX 77004, USA

9   [3]Cyprus Subsea Consulting and Services, Lakatamia 2326, Cyprus

10   [4]now at Akvaplan-Niva, 9296 Tromsø, Norway

11   [5] -4H-JENA engineering GmbH, 07745 Jena, Germany

12   [6] College of Fisheries and Ocean Science, University of Alaska Fairbanks, Fairbanks, AK 99775,

13   USA

14   [7]now at Alaska Renewables, Fairbanks, AK 99709, USA

15

16   Corresponding author: Claudine Hauri (chauri@alaska.edu)

Abstract

Warming, ocean acidification, and deoxygenation are increasingly putting pressure on marine ecosystems. At the same time, thawing permafrost and decomposing hydrates in Arctic shelf seas may release large amounts of methane (CH_4) into the water column, which could accelerate local ocean acidification and contribute to climate change. The key parameters to observing and understanding these complex processes and feedback mechanisms are vastly undersampled throughout the oceans. We developed carbon dioxide (CO_2) and CH_4 gliders, including standard operational procedures with the goal that CO_2 and CH_4 measurements become more common for glider operations. The Seagliders with integrated Contros HydroC CO_2 or CH_4 sensors also include conductivity, temperature, depth, oxygen, chlorophyll-a, backscatter, and fluorescent dissolved organic matter sensors. Communication via satellite allows for near-real time data transmission, sensor adjustments, and adaptive sampling. Several sea trials with the CO_2 Seaglider in the Gulf of Alaska and data evaluation with discrete water and underway samples suggest near 'weather quality' CO_2 data as defined by the Global Ocean Acidification Network. A winter mission in Resurrection Bay, Alaska provided first insights into the water column inorganic carbon dynamics during this otherwise undersampled season. The CH_4 Seaglider passed its flight trials in Resurrection Bay, yet needs to be tested during a field mission in an area with CH_4 concentrations beyond background noise. Both sensing systems are available to the science community through the industry partners (Advanced Offshore Operations and -4H-JENA engineering GmbH) of this project.

1. Introduction

39   Understanding the distribution and dynamics of carbon dioxide (CO_2) and methane (CH_4)

40   in the ocean is crucial for predicting and mitigating climate change and ocean acidification

41   impacts. Within the ocean, CO_2 levels (measured as the partial pressure of CO_2, pCO_2 and/or

42   fugacity of CO_2) are spatially and temporally variable as they are influenced by a myriad of

43   highly dynamic physical, chemical, and biological processes. On top of this natural variability,

44   the ocean has absorbed about one third of the CO_2 emitted by humans since the industrial

45   revolution (Sabine et al., 2004; Gruber et al., 2019). In doing so, it has played an important role

46   in mitigating climate change (Sabine and Tanhua, 2010). However, both the oceanic uptake of

47   anthropogenic CO_2 and climate change are altering the distribution of oceanic CO_2 and are

48   causing ocean acidification (Doney et al., 2009; Qi et al., 2022; Woosley and Millero, 2020). At

49   the same time, the oceans are warming and losing oxygen (Johnson and Lyman, 2020; Breitburg

50   et al., 2018), increasing the stress on marine ecosystems. As these long-term changes unfold,

51   marine heat waves, and high acidity or low oxygen extreme events will last longer, become more

52   intense, and happen more often and at the same time (Laufkötter et al., 2020; Gruber et al., 2021;

53   Hauri et al., 2024). Negative effects on certain organisms are even stronger if exposed to a

54   combination of different stressors (Breitberg et al., 2015; Kroeker et al., 2017).

55   Over the coming 100 years, CH_4 possesses a global warming potential approximately 28

56   times greater than that of CO_2 (IPCC AR5; Myhre et al., 2013). Sediments along the seafloor at

57   continental margins contain large amounts of CH_4, with about ten times as much carbon as the

58   atmosphere (Kessler, 2014). CH_4 is biologically produced in anoxic sediments and the surface

59   mixed layer or released from geological sources like hydrocarbon seeps and degrading methane

60   hydrate deposits (Barnes and Goldberg; Du et al, Skarke 2014). This powerful greenhouse gas is

61   emitted to the atmosphere through bubbling (ebullition) or diffusive gas transfer (Reeburgh,

62 2007; McGinnis et al., 2006), which is limited by rapid oxidation to CO_2 during transport

63 through the water column (Leonte et al., 2017). CH_4 occurs generally at low levels (background

64 concentrations) throughout oceans, unless close to a source. Positive feedback mechanisms, like

65 warming induced CH_4 seepage from destabilizing hydrates and thawing subsea permafrost, may

66 further accelerate ocean acidification and climate change (Garcia-Tigreros et al., 2021; Sparrow

67 et al., 2018; Shakhova et al., 2010; Rees et al., 2022).

68   To effectively observe and understand the complex processes and feedback mechanisms

69 regulating Earth's systems, certain key parameters, defined by the Global Ocean Observing

70 System as essential ocean variables, must be measured accurately. However, these variables are

71 often vastly undersampled across time and space due to traditional sampling methods, which rely

72 mainly on discrete water sample collections from dedicated research cruises, underway

73 measurements from transiting vessels, or time series measurements from in situ sensors on fixed

74 moorings. Although biogeochemical sensors deployed on autonomous platforms like moorings

75 and Argo floats have become more prevalent, challenges such as high power requirements,

76 sensor size, and data quality hinder their widespread use on underwater gliders. Autonomous,

77 spatially resolved surface measurements of $p$$CO_2$ and pH are commonly collected using wave

78 gliders and sail drones (Chavez et al., 2018; Nickford et al., 2022; Manley and Willcox, 2010).

79 The state-of-the-art biogeochemical (BGC) Argo floats measure variables like pH, O_2, NO_3,

80 chlorophyll-a, suspended particles, and downwelling irradiance in subsurface waters (Claustre et

81 al., 2020). These floats can last several years at low sampling resolutions, such as a 2000-meter

82 depth profile every ten days, or they can be programmed for high-resolution and shallow

83 sampling. They can even sample beneath seasonal sea ice (Briggs et al., 2018). Despite their

84　　capabilities, their trajectory is hard to control, and they are usually not recovered after their

85　　mission, which prevents sensor calibration and post-mission corrections.

86　　　　　Ocean gliders autonomously collect water column data along planned waypoints, which

87　　allows for controlled exploration and adaptive sampling. To date, pH is the only carbon system

88　　parameter that has been successfully integrated into ocean gliders (Hemming et al., 2017; Saba et

89　　al., 2019; Possenti et al., 2021; Takeshita et al., 2021). The most promising results came from

90　　ISFET based pH sensors (Saba et al., 2019; Wright-Fairbanks et al., 2020; Takeshita et al.,

91　　2021). However, ISFET-based pH sensors require significant conditioning periods before

92　　deployment, suffer from biofouling, require annual cleaning and calibration at the manufacturer,

93　　and careful discrete sample collection at deployment and recovery to characterize and correct for

94　　sensor drift (Thompson et al., 2021). There have been few attempts to integrate pCO_2 sensors

95　　into gliders (Hemming et al., 2017; Hauri et al., 2018; von Oppeln-Bronikowski et al., 2021).

96　　Hemming et al. (2017) did not publish the data because of low quality. Von Oppeln-Bronikowski

97　　et al. (2021) integrated an Aanderaa CO_2 optode that measures pCO_2 by detecting the

98　　luminescent quenching response from a CO_2-sensitive membrane with a Slocum G2 glider but

99　　suffered from instability, thermal-lag issues, variable conditioning periods (4 days to 1 month),

100　　large offsets (> 1000 uatm), nonlinear temperature-dependent response time, and a high

101　　dependence on prior foil calibration. Hauri et al. (2018) integrated the Pro Oceanus Mini Pro

102　　CO_2 sensor with a Slocum G2. However, the Pro Oceanus Mini Pro CO_2 sensor used at the time

103　　did not withstand the pressure changes imposed by glider missions. The Franatech METS CH_4

104　　sensor has been integrated into Alseamar SeaExplorer and Teledyne Slocum gliders and

105　　successfully used to generate concentration maps of a methane seep in a semi-quantitative way

106　　(Meurer et al., 2021).

107   Here we integrated modified versions of the Contros HydroC CO_2 and CH_4 sensors with

108   a Seaglider® (registered trademark of the University of Washington). We discuss details of the

109   physical and software integration, present CO_2 and CH_4 data from tank experiments, evaluate the

110   quality of $p$$CO_2$ data collected during CO_2 Seaglider missions, and discuss highlights from

111   missions in Resurrection Bay, Alaska.

112

113   **2. Methods**

114   2.1 CO_2 Seaglider

115   We integrated a modified version (Seaglider (SG) HydroC CO_2) of the CONTROS

116   HydroC^{TM} CO_2 sensor (-4H-JENA engineering GmbH, Kiel, Germany) with a Seaglider M1

117   (Figure 1 a and b). The Seaglider M1 was specifically designed for long endurance missions in

118   deep waters to 1000 m depth. The HydroC CO_2 sensor was outfitted with a semi-permeable

119   TOUGH membrane (Pinnau and Toy, 1996) that equilibrated dissolved CO_2 between the ambient

120   seawater and the headspace of the sensor, where the gas concentration was determined by

121   nondispersive infrared (NDIR) spectrometry.

122   Since the equilibration time (response time) of membrane-based sensors is affected by the

123   exchange of the water mass in front of the sensor head, we installed a Seabird Electronics (SBE)

124   5M pump next to the SG HydroC CO_2 sensor using tubing to transfer seawater from outside the

125   glider fairing to the membrane surface (Figure 1a). The response time was determined at the

126   manufacturer, verified in the field, and then used to correct for hysteresis during the post-

127   processing phase (see Section 2.7.2).

128   The form factor of the HydroC CO_2^{TM} sensor and Seaglider were changed to achieve an

129   internal integration of the sensor with the Seaglider. The standard high-performance HydroC

130   CO_2^{TM} sensor was changed from ⌀ 89 x 380 mm to ⌀ 136 x 294 mm by rearranging the gas-cycle

131   components and the control unit (Figure 1c). This new SG HydroC CO_2 sensor is available in

132   polyoxymethylene cladding rated to 300 m or a titanium housing rated to 1000 m to provide a

133   choice between a coastal mission and an offshore deeper mission. Use of the titanium housing

134   required a syntactic foam housing to compensate for the weight, whereas the polyoxymethylene

135   housing was integrated into the glider with simple brackets (Figure 2). Despite these adjustments

136   to the size of the sensor, to our knowledge, it is still the largest and heaviest sensor that has been

137   integrated with a Seaglider to date. The forward fairing of the Seaglider was extended by 40 cm

138   with a fiberglass cylindrical extension to create internal wet payload space for the sensor, pump,

139   and cables (Figure 1 a and b). The sensor was mounted with the membrane facing aft to ensure

140   that potential bubbles within the internal tubing of the sensor could escape the system during the

141   downcast of the first dive. In situ comparison of the orientation of the sensor and close

142   examination of pCO_2 and internal pressure data suggested the highest data quality was achieved

143   with this mounting design.

144   One of the advantages of using ocean gliders for ocean observing is the ability for real-

145   time communication of data and commands between the pilot and the glider. To take advantage

146   of this, modifications were needed to allow two-way communication between the Seaglider

147   firmware and the HydroC firmware. The Seaglider firmware has a feature to allow easy

148   integration of "logging devices," which provides a way to build commands for the pilot on land

149   to switch the sensor on and off and change sampling strategy during the mission (on/off below or

150   above certain depth) when it comes to the surface for a communication session. The Seaglider

151   firmware can also automatically set the clock of the sensor on request at every surfacing and

152   send small samples of the data stream via Iridium along with the standard sensor data. This

7

153   required the writing and testing of a driver file (CNF file). However, to take full advantage of the

154   ability of the HydroC, a more-advanced electronic integration was carried out using Smart

155   Interoperable Real-time Maritime Assembly (SIRMA™, registered trademark of Cyprus Subsea

156   Consulting and Services, C.S.C.S., Ltd.). This small programmable electronic circuit contained

157   hardware elements to adapt the sensor power and communication requirements to those available

158   on the host platform. It also allowed for separate storage and processing capabilities to

159   supplement the main host processor that controls the flight, sampling, and telecommunications of

160   the host. Most importantly here, it was programmed to relay pilot commands to the SG HydroC

161   CO_2 for the built-in "zero" function, which isolated the internal gas circuit until there was no

162   CO_2 present, measured the concentration signal, and assigned a zero value. Then the gas circuit

163   was exposed to the headspace behind the diffusion membrane for in situ sampling. SIRMA was

164   also programmed to extract raw data from the HydroC and calculate the bin average of some of

165   the output fields, which were useful for real-time mission adaptation and confirmation of sensor

166   operation. Three levels of output were allowed, depending on how much surfacing time could be

167   tolerated before continuing the mission (Baud rate for Iridium is very low, on the order of 4800

168   bps). More detailed information can be found in the CO_2 Seaglider SOP (Irving et al., 2024).

169   In addition to the HydroC CO_2 sensor, the CO_2 Seaglider carried an Aanderaa 4831F

170   optode, a compact optical oxygen sensor, which works on the principle of luminescence

171   quenching by oxygen with a precision of 0.1 μM and an absolute accuracy of +/- 2 μM after

172   multipoint calibration. The 4831F was equipped with a fast response sensing foil with a well-

173   characterized response time of 8 seconds. The Aanderaa optode measured absolute oxygen

174   concentration and percentage saturation. It is the most widely used on ocean gliders and has been

175   integrated into both Slocum and Seagliders (OceanGliders Oxygen SOP, 2024; Bittig et al.,

176   2018). The OceanGliders community has developed a Standard Operating Procedure (SOP) that

177   details everything from mounting, calibration, available sensors, piloting tips, and response time

178   correction, to post-processing (OceanGliders Oxygen SOP, 2024). The CO_2 Seaglider was also

179   outfitted with an SBE CT sail and Wetlabs Ecopuck measuring chlorophyll fluorescence at 695

180   nm.

181

182   **2.2 CH_4 Seaglider**

183   We also integrated a modified version of the CONTROS HydroC CH_4 sensor (-4H-JENA

184   engineering GmbH, Kiel, Germany) with the Seaglider. The manufacturer's published

185   uncertainty of the HydroC CH_4 sensor is 2 μatm or ± 3 %, whichever is greater . The SG HydroC

186   CH_4 sensor had the same form factor as the SG HydroC CO_2 sensor. However, it was 0.5 kg

187   heavier due to its Tunable Diode Laser Absorption Spectroscopy (TDLAS) component, so the

188   SG HydroC CH_4 had to be integrated with changes to the glider's ballast.

189

190   **2.3 Spring and winter CO_2 Seaglider missions**

191   Both versions of the CO_2 Seaglider (rated to 300 m versus 1000 m) were tested in

192   separate missions (Figure 3, Table S1) in spring (53 dives, 4 – 7 May 2022, Figure 4) and winter

193   (310 dives, 8 – 21 February 2023, Figure 5). The 300 m version with integrated

194   polyoxymethylene housing was tested during the 4 – 7 May 2022 mission. The glider followed

195   along a transect within Resurrection Bay. CTD casts near the glider path allowed for in-depth

196   evaluation of the data quality. The 1000 m depth-rated CO_2 Seaglider with integrated titanium

197   housing was tested in February 2023. Estimated energy consumption during the CO_2 Seaglider

198   missions was 19 out of 135 Ah and 75 out of 120 Ah for the 24 V which powered the SG

199   HydroC CO_2 sensor battery for the spring and winter missions, respectively. Before the February

200   mission, the on board modem was replaced with a newer model, with different input voltage

201   requirements, which were probably not met as the mission evolved. As a result, the glider could

202   not communicate and was lost. While this was an unfortunate mistake, the loss of the glider had

203   nothing to do with the HydroC CO_2 integration.

204

205   **2.4 Tank experiments**

206   Shortly before the May 2022 glider mission, the glider was kept in a flow-through tank at

207   the Alutiiq Pride Marine Institute for roughly 12 h for cross-calibration purposes. The flow-

208   through tank was fed with water from about 75 m depth and 91 m from the laboratory into

209   Resurrection Bay, near a freshwater source. During the tank experiment, SG HydroC CO2T-

210   0718-001 (Figure 6b, blue line) was integrated into the Seaglider, and SG HydroC CO2T-0422-

211   001 (Figure 6b, black line) and the SG HydroC CH_4 (Figure 6c) sensors were secured next to the

212   Seaglider. The water was kept in motion with a circulation pump. Triplicate discrete water

213   samples for dissolved inorganic carbon, pH, and CH_4 analysis were taken every four hours

214   (Table 1).

215

216   **2.5 Rosette package**

217   One of the SG HydroC CO_2 sensors (CO2T-0422-001) was installed on an SBE-55 frame

218   ECO water sampler with six 4-liter sample bottles (Seabird Scientific) during the May 2022 trials

219   (Tables 2 and 3, Figure 7 and S1). The SBE-55 and SG HydroC CO_2 were powered by an SBE-

220   33 carousel deck unit. The SG HydroC CO_2 interfered with the communication stream and

221   thereby prevented real-time data acquisition and control of the SBE-55, however data were

222 internally logged. The depth of the rosette package was monitored directly on the winch and the

223 timing of firing of the sample bottles, after an approximate 15-minute hovering period (to allow

224 for equilibration), was programmed in advance based on time intervals. On May 3 (Table 2,

225 Figure 7) only samples from the upper 20 m of the water column were usable due to issues with

226 manually measuring the depths and the sample collection. On May 7 (Table 3, Figure S1) two

227 bottles that were intended to be fired while the rosette was stationary at depth, were instead fired

228 while the rosette was in motion.

229

230 **2.6 Discrete water samples**

231 2.6.1 Inorganic carbon chemistry

232   Discrete seawater samples were collected for sensor validation in two different cases in

233 May of 2022. Firstly, samples were taken alongside two SG HydroC CO_2 sensors during a tank

234 experiment at the Alutiiq Pride Marine Institute (Figure 6b, Table 1), from adjacent sample

235 bottles (Figure 1d). Secondly, samples were taken from bottles during a CTD cast within 1 km

236 and 4 hours of the HydroC measuring pCO_2 on the glider while conducting dives (Section 3.2).

237   Inorganic carbon sampling in the Gulf of Alaska's glaciated coastal regions required

238 methodological variations from open-ocean best practices to ensure that suspended mineral

239 particles do not compromise the instrumentation and/or bias measurements between sample

240 collection and analysis (Sejr et al., 2011). Given this, the discrete seawater samples were filtered

241 (replaceable 0.45 µm filter in a 47 mm polycarbonate in-line filter) with a peristaltic pump

242 straight from the Niskin bottles (see Bockmon and Dickson (2014) for detailed method), or tank,

243 into pre-cleaned 500 mL borosilicate bottles, and poisoned with 200 µL mercuric chloride

244 ($HgCl_2$) (Dickson et al., 2007). Samples were transported and stored at room temperature before

245   analysis. Samples were opened immediately (< 10 minutes) before concurrent analyses of pH

246   and DIC to limit gas exchange with ambient lab conditions. Samples were analyzed for DIC

247   using an Apollo SciTech, LLC Dissolved Inorganic Carbon Analyzer model AS-C6. All species

248   of dissolved inorganic carbon in a sample were converted to CO_2 by the addition of a strong acid.

249   The CO_2 gas was then purged from the sample through a drying system. The concentration of

250   CO_2 gas was measured using a non-dispersive infrared gas analyzer, the LI-7000 CO_2/H_2O

251   Analyzer. This method required Certified Reference Material (CRM, Batch #198 from A.

252   Dickson's Certified Reference Materials Laboratory) to create a three-point calibration line. The

253   calibration line was used to quantify the total amount of CO_2 in the sample as the integrated area

254   under the concentration-time curve. Apollo SciTech recommendations to improve analytical

255   accuracy were followed and included bubbling of CO_2 off the acid daily, allowing the analyzer to

256   warm up for at least 2 hours before measurements begin, measuring a set of standards at the

257   beginning and end of each day and every 9 samples, using Ultra High Purity (UHP) N_2 gas, and

258   filtering the N_2 gas with a PTFE filter, CO_2 scrubber (Ascarite II) and H_2O scrubber

259      $(Mg(ClO_4)_2)$.

260   Samples were analyzed spectrophotometrically for pH with a CONTROS HydroFIA pH

261   (Aßmann et al., 2011) operating in discrete measurement mode using unpurified m-Cresol Purple

262   (mCP) as the indicator dye (Clayton and Byrne, 1993). Sample temperature was stabilized

263   at 25.00 +/- 0.01 °C during measurements using Peltier elements and 5 repetitive measurements

264   were taken for each sample. At the beginning of each day, the HydroFIA pH underwent a

265   conditioning period using seawater with similar properties until values stabilized. CRMs (known

266   TA and DIC concentration, Batch #198 from A. Dickson's Certified Reference Materials

267   Laboratory) were measured at the beginning and end of the day, as well as every 9 samples.

268   All data processing and analyses were done using an in-house MATLAB routine. In situ

269   pH and pCO$_2^{disc}$ were calculated from input pair pH$_{lab}$ and DIC using CO2SYSv3 (Sharp et al.,

270   2023) with dissociation constants for carbonic acid of Sulpis et al. (2020), bisulfate of (Dickson,

271   1990), hydrofluoric acid of Perez and Fraga, (1987), and the boron-to-chlorinity ratio of (Lee et

272   al., 2010). Sulpis et al. (2020) found that the carbonic acid dissociation constants of Lueker et al.

273   (2000) may underestimate pCO$_2$ in cold regions (below ~8°C) and, therefore, overestimate pH

274   and CO$_3^{-2}$. Differences between discrete pCO$_2$ calculated with the carbonic acid dissociation

275   constants by Lueker et al. (2000) (the standard in synthesis data products (e.g., Jiang et al., 2021,

276   Lauvset et al., 2022, Metzl et al., 2024) and the HydroC pCO$_2$ from the tank experiment were

277   found to be on average 4.6 µatm (1.6 %) and 4.2 µatm (0.7 %) greater for SN0422 and SN0718,

278   respectively, when compared with discrete pCO$_2$ based on carbonic acid dissociation constants

279   by Sulpis et al. (2020).

280   Discrete pCO$_2$ uncertainty (u$_c$) was calculated as the combined standard uncertainty from

281   *errors.m* (Orr et al., 2018) that propagates input uncertainties plus errors in the dissociation

282   constants. Input uncertainties for pH$_{lab}$ and DIC were the standard uncertainties, defined as the

283   square root of the sum of the squared random uncertainty component plus the squared systematic

284   uncertainty components. For pH$_{lab}$ the random uncertainty was the sample precision, or standard

285   deviation of the measurements. For DIC, the random uncertainty was the propagated error

286   calculated with the first-order Taylor series expansion (Equation 1, Orr et al. (2018)) and

287   assuming the correlation term was zero for the conversion of molarity (µmoles l^{-1}) to molality

288   (µmoles kg^{-1}). Systematic uncertainty components were the uncertainty in the CRM used for

289   instrument offset and drift correction, and the published instrument accuracy, or if available, the

290   daily instrument accuracy as defined below. Daily instrument accuracy was defined as the

13

291   maximum difference between the known CRM concentration, and the measured CRM

292   concentration after data were corrected for instrument drift and offset of all available CRM's not

293   used in the instrument drift and offset calculation. CRM pH_{lab} "known" values were calculated

294   using CO2SYSv3 (Sharp et al., 2023) with inputs pH and DIC. Nutrient concentrations (SiO_4^{-2},

295   PO_4^{-3}) were assumed to be negligible in the CO2SYS calculations (e.g. DeGrandpre et al., 2019;

296   Vergara-Jara et al., 2019; Islam et al., 2017).

297

298   2.6.2 Methane

299   Two sets of triplicate pCH$_4$ discrete water samples were collected during the tank

300   experiment for an initial evaluation of the SG HydroC CH$_4$ sensor (Table 1, Figure 6c). Seawater

301   was filtered from the tank into 250 mL vials. The vials were closed with a rubber stopper, topped

302   with an aluminum cap, and closed with a crimp immediately. A dry and clean syringe was

303   flushed with 10 mL of N_2 gas twice. The third fill was kept, and the syringe valve was closed. N_2

304   was then injected into the headspace while simultaneously pulling 10 mL seawater out of the vial

305   using a second syringe. 50 μL mercuric chloride ($HgCl_2$) were added to the vial, which was then

306   shaken for about a minute and put into a fridge at 4°C for over 12 h to equilibrate the headspace.

307   The samples were then sent to the Kessler analytical laboratory at the University of Rochester for

308   analysis.

309

310   **2.7 Data post-processing**

311   *2.7.1 pCO$_2$ post-processing*

312   SG HydroC CO$_2$ data were post-processed using Jupyter Notebook scripts developed by -4H-

313   JENA engineering GmbH at the original resolution (2 seconds). SG HydroC CO$_2$ (SG HydroC

14

314   CO2T-0422-001) data from the tank experiment (Table 1, Figure 6) and rosette mounted CTD

315   casts (Table 2 and 3, Figure 7 and S1) were post-processed to correct for baseline drift (change in

316   the zero signal reference) and span drift (changes in the sensor's concentration dependent

317   characteristics) using pre- and post-calibration coefficients interpolated over the

318   deployment (Fietzek et al., 2014). For the May 2022 Seaglider integrated SG HydroC

319   CO_2 sensor (SG HydroC CO2T-0718-001, Table 3, Figures 4 and 8), data were post-processed

320   with pre-calibration coefficients only (no span drift correction) because the sensor was damaged

321   during the return shipment for post-calibration. Differences between sensors remained low

322   despite the difference in processing, with a mean difference during the tank experiment of 2.1 $\pm$

323   1.0 µatm (0.9%) and median difference of 2.0 $\pm$ 1.0 µatm (0.9%) (Table 1, Figure 6b).

324   The pCO$_2$ data from February 2023 was collected with a sensor that was factory calibrated two

325   weeks prior to deployment (SG HydroC CO2T-0422-001) but were not post-processed because a

326   required parameter (p_NDIR) was not relayed in real-time and the glider was lost. Lack of post-

327   calibration most likely had no negative effect on the quality of data since the HydroC was only

328   collecting data for ~4 days during the spring mission and ~2 days during the winter mission.

329   HydroC pCO$_2$ and pCO$_2^{RTC}$ data at the original resolution (2 s) and RTC resolution (8 s)

330   were linearly interpolated onto the Seaglider timestamp and 1-meter binned data were calculated

331   by first averaging 1 meter (+/- 0.5 m) upcast and downcast data independently, linearly

332   interpolating over gaps, then averaging the interpolated 1-meter binned upcast and downcast

333   together.

334

335   *2.7.2 Response time correction*

336   The ability to determine the in situ response time (τ_{63} of the HydroC, which took into

337   account membrane characteristics and the rate of water exchange over the membrane, i.e.

338   pump characteristics) of the sensor made correction for hysteresis through data post processing

339   possible. This is critical for a sensor operating on profiling platforms, especially in the Gulf of

340   Alaska, where strong environmental gradients were encountered. Fiedler et al. (2013) used a

341   CONTROS HydroC^{TM} CO_2 with a silicone, polydimethylsiloxane (PDMS) membrane and

342   reported a linear response time dependency on water temperature on the order of one second per

343   one °C. For this study, the SG HydroC CO_2 sensors were deployed with the new robust TOUGH

344   membrane, which had Teflon AF2400 as the active separation layer with a low temperature

345   dependence on the permeability coefficient (Pinnau and Toy, 1996). Response times determined

346   during calibration at -4H-JENA were used for response time correction (RTC) and found to be

347   106 seconds for the HydroC mounted on the rosette in May 2022 and 108 seconds when it was

348   integrated into the Seaglider in February 2023 (HydroC CO2T-0422-001). The response time of

349   the HydroC integrated into the Seaglider in May 2022 (HydroC CO2T-0718-001) was 109

350   seconds. Since field verification of the response time was recommended to ensure the highest

351   quality post-processed data product (because τ_{63} can be affected by the speed of water exchange

352   across the membrane due to pump speed, tube length, etc.), we verified the sensor response time

353   at deployment. After the glider was stationary for approximately 15 minutes, a zeroing interval

354   was performed with the HydroC CO_2. The response time was determined by reviewing the time

355   it took for the signal to recover to the ambient concentration. Our in situ response time tests were

356   suggested to be within 5 seconds of the response time found during calibration (not shown).

357   Before RTC was applied, HydroC CO_2 data were smoothed using a quadratic regression

358   (MATLAB's smoothdata.m function with the loess method) over a 2-minute window. This was

359   done to eliminate erroneous spikes in the RTC signal while retaining the original 2-second

360   resolution of the $p\text{CO}_2$ data. The RTC resolution of 8 seconds was determined with the L-curve

361   analysis included in the publicly available code from Dølven et al. (2022). The Dølven et al.

362   (2022) RTC method was used because it produced more realistic profiles than an RTC method

363   (Miloshevich et al., 2004, not shown) previously used for HydroC CO_2 correction from a

364   profiling float (Fielder et al. 2013). In addition, Dølven et al. (2022) developed their algorithm

365   with equilibrium-based sensors in mind and was proven with a sensor with a long response time

366   (HydroC CH4 $\tau_{63} \cong 23$ minutes).

367

368   *2.7.3 pCH4 post-processing*

369   SG HydroC $p\text{CH}_4$ data were response time corrected using a τ_{63} of 43 minutes (Dølven et

370   al., 2022; Figure6c, blue line). Before RTC was applied, HydroC CH4 data were smoothed using

371   a quadratic regression (MATLAB's smoothdata.m function with the Loess method) over a 2-

372   minute window to avoid erroneous spikes in the RTC data while retaining the original 2-second

373   resolution of the $p\text{CH}_4$ data. The RTC resolution of 30 seconds was determined with the L-curve

374   analysis included in the publicly available code from Dølven et al. (2022). Discrete CH4 samples

375   were collected during the tank experiment (Table 1, Figure 6c red diamonds) and analyzed at

376   John Kessler's laboratory at the University of Rochester. Discrete CH4 sample values were

377   converted from the concentration of dissolved gas in water (mol L^{-1}) to partial pressure ($p\text{CH}_4^{\text{disc}}$,

378   µatm) using the solubility coefficient following Sarmiento and Gruber (2006). $p\text{CH}_4^{\text{disc}}$

379   uncertainty (u; Table 1, Figure 6c red error bars) was calculated as the square root of the sum of

380   the squared 1) mean of the standard deviations from each sample as returned from the lab and 2)

381   the standard deviation of the triplicates.

382

3. Results

3.1 Glider flight

The Seaglider was able to "fly" properly, allowing the desired undisturbed flow, despite the large payload and major changes to the vehicle fairing. Example flight profiles with the polyoxymethylene and Titanium integrated sensors are shown in Figures 9 and 10, respectively. Pitch and vertical velocity are in the stable range, and roughly symmetric between downcast and upcast, indicating a nearly balanced glider. Heading varies around the targeted value as the roll adjusted to heading errors. It should be noted that this level of variability is typical of standard Seagliders. Operating Seagliders in shallow water (< 200 m) is risky because of the likelihood of meeting depth-averaged currents of the same order of magnitude as the vehicle speed. A typical single dive cycle of downcast and upcast shows that the sensor data are free of noise that could be expected if there were recirculated water from the glider meeting the sensors. The expected endurance of the CO_2 Seaglider is around 18 days and 15 days for the CH_4 Seaglider with constant sampling at full depth.

3.2 CO_2 Seaglider data evaluation

The quality of the CO_2 Seaglider data was thoroughly tested with discrete measurements during a tank experiment, nearby CTD cast, and glider missions.

3.2.1 Tank experiment

Discrete water samples show good agreement with the SG HydroC CO_2 sensors (Figure 6b, Table 1). The values of discrete water samples represent the average of triplicate samples

18

405 (Figure 6c, red diamonds). Differences between the SG HydroC CO_2 sensors remained low, with

406 a mean difference during the tank experiment of 2.1 ± 1.0 µatm (0.9 %) and median difference of

407 2.0 µatm (0.9 %; Table 1). Percent differences (Eq. 1) between the SG HydroC CO_2 sensors and

408 discrete water samples collected in the tank were between -1.4 and 1.9 % (Table 1, Figure 6).

409 $\% \ difference \ = \frac{pCO_2{}^{HydroC} - pCO_2{}^{disc}}{pCO_2{}^{disc}} * 100\%$ (Equation 1)

410

411 3.2.2 Profiling experiment

412   Rosette-based profiles with the SG HydroC CO_2 sensor in combination with discrete

413 water samples were used to test and evaluate the response correction algorithm by Dølven et al.

414 (2022). The rosette was lowered into the water and kept at different depths for about 20 minutes

415 at a time (Figure 7a and Figure S1a). Sample bottles were programmed to collect seawater

416 toward the end of each hovering period. pCO$_2$ measured with the HydroC ranged from 218 µatm

417 at the surface to 411 µatm at 80 m depth on 3 May (Figure 7b) and 231 µatm at the surface to

418 382 µatm at 77 m depth on 7 May (Figure S1). Differences between the rosette mounted SG

419 HydroC CO_2 sensor and discrete samples ranged from -3.3 µatm (-1.4 %) to 8.2 µatm (3.5 %)

420 with a lowest percent difference of 0.6 % (Table 2) on 3 May and from -5.7 µatm (-1.6 %) to

421 12.1 µatm (3.9 %) with a lowest percent difference of 0.3 % (Table 3) on 7 May.

422

423 3.2.3 Data evaluation during CO_2 Seaglider mission

424   The quality of the pCO$_2$ data from the CO_2 Seaglider was further evaluated during a 4 – 7

425 May sea trial mission in spring 2022 in Resurrection Bay, Alaska (Figure 3).

426 Discrete water samples were taken in proximity (1 km and within 4 hours) of the downcast of

427 dive #51 (Table 3, Figures 4a and 8). The response time corrected CO_2 Seaglider data compares

428 well with the discrete water samples (Figure 8), overestimating the discrete water samples

429 between 8.3 µatm (2.7 %) and 12.0 µatm (5.1 %) (Table 3). The mean difference between the

430 rosette mounted and Seaglider integrated SG HydroC CO_2 sensors during the 7 May cast at the

431 time of discrete samples was 8.5 µatm +/- 8.9 µatm (3.7 %). The larger difference between SG

432 HydroC CO_2 sensors compared to the difference during the tank experiment (see Section 3.2.1)

433 is unsurprising, given the spatial and temporal distance between sensors (Table 3). Collecting

434 more discrete samples throughout the water column and in closer proximity (within 100 m,

435 Thompson et al., 2021) to the CO_2 Seaglider conducting dives would allow a more tightly

436 constrained uncertainty estimate for response time corrected pCO_2 data collected on a glider and

437 should be a priority for future researchers.

438

439 **3.3 CH_4 Seaglider data evaluation**

440 3.3.1 Tank experiment

441   The SG HydroC CH_4 was also evaluated during the tank experiment described in section

442 2.4 (Figure 6c). Percent differences (Eq. 1) between discrete pCH_4 (average of triplicate samples)

443 and pCH_4^{RTC} were 6.6 to 15.8 % (Table 1). During the experiment, there was a decrease in

444 salinity from 30.95 to 29.88 where pCO_2 decreased by 80 µatm. The corresponding pCH_4^{RTC}

445 signal decreased by 25.4 µatm from 32.3 to 6.9 µatm. Although the triplicate discrete pCH_4 water

446 samples were slightly lower than the sensor-measured pCH_4 values, they also reflected this step

447 change.

448

449 **3.4 Winter and springtime pCO_2 in Resurrection Bay, Alaska**

450   The surface-to-subsurface pCO_2 gradient is much larger in spring than in winter (Figure

451 11). During the 4 – 7 May mission, the average surface $pCO_{2,Seaglider}^{RTC}$ was 240.7 +/- 16.5 µatm

452 (mean +/- standard deviation at 2 meters) with an average temperature of 5.8 +/- 0.4 °C (Figures

453 4 and 11). In February, surface $pCO_{2,Seaglider}^{RTC}$ was near atmospheric pCO_2 (427.4 +/- 13.0 µatm,

454 temperature 4.1 +/- 0.3 °C) and about 180 µatm higher than in May (Figures 5 and 11). NOAA's

455 moored sensor located in Sunny Cove (59.911 °N, -149.35 °W), near the CO_2 Seaglider trial site,

456 measured an average sea surface pCO_2 of 240.7 +/- 10.4 µatm during the time of the May 2022

457 mission (Monacci et al., 2023), which compared remarkably well with the Seaglider based

458 measurements. A minimum of 140 µatm was measured in Sunny Cove in mid-April (3-day

459 average) (Figure 12, Monacci et al., 2023), suggesting that the peak of the spring bloom

460 happened three weeks before the May 2022 glider mission. Since we don't have salinity data

461 from the May CO_2 Seaglider mission (conductivity sensor failure), we cannot disentangle the

462 contributions of freshwater or primary production on the low surface pCO_2 values observed

463 (Figure 4). The moored sensor in Sunny Cove measured an average sea surface pCO_2 of 416.4

464 +/- 4.2 µatm during the time of the February mission, straddling the atmospheric pCO_2 values

465 (Monacci et al., 2023, Figure 12). Subsurface $pCO_{2,Seaglider}^{RTC}$ at 180 m was on average 545.6 +/-

466 16.9 µatm during the February mission and 518.2 +/- 37.4 µatm during the May 2022 mission

467 (Figure 11a). pCO_2 was much lower in May than in February throughout the upper water column

468 (< 120 m), whereas there was not much of a seasonal difference at deeper depth. Some of the

469 fine scale features apparent in the May pCO_2 and O_2 profiles are likely due to various levels of

470 photosynthetic activity (Figure 11). As the glider transitioned into the open Gulf of Alaska

471 during the February mission, water with $O_2 < 150$ µM shoaled into the upper 150 m of the water

472   column (Figure 5). Unfortunately, the HydroC CO_2 sensor was turned off at that stage of the

473   mission to conserve battery.

474

475   **4. Discussion**

476   The newly developed CO_2 Seaglider is the first of its kind to autonomously collect high

477   quality pCO_2 data. The tank and rosette experiments and in situ data evaluation suggest that the

478   post-processed data from the CO_2 Seaglider generally fall near the relative uncertainty of 2.5%,

479   which is a threshold defined as the "quality sufficient to identify relative spatial patterns and

480   short-term variation" ("weather quality", Newton et al., 2015). This is the highest quality of

481   pCO_2 data that has been measured with a subsurface autonomous vehicle to this date and

482   therefore an important step towards filling the subsurface carbonate system data gap. -4H-JENA

483   is reassessing their sensor calibration methodology and data post-processing algorithm to further

484   improve the HydroC's data accuracy.

485   The newly developed CO_2 Seaglider is suitable for data collection in open ocean or

486   coastal environments with bottom depths deeper than 300 m. However, the coastal Gulf of

487   Alaska is a highly dynamic environment, with strong freshwater and wind influence, and rugged

488   shallow (often < 200 m) bottom topography. Strong currents (up to 0.50 m s^{-1}) made the piloting

489   of the glider extremely difficult throughout the project and confirmed that the Seaglider cannot

490   reliably reach desired waypoints in these conditions. The current version of the CO_2 Seaglider is

491   also not suitable for operating in the coastal Gulf of Alaska in summer and early fall, due to

492   strong seasonal salinity gradients in this freshwater influenced area. Another issue we faced was

493   the fact that the forward-looking altimeter could not detect the Seafloor as it should in its

494   position behind the HydroC CO_2. In areas with detailed topography maps this would not be an

22

495   issue, but in the coastal Gulf of Alaska reliable topography information is not readily available

496   yet. An obvious next step is to integrate the SG HydroC CO_2 sensor into a newer glider platform,

497   such as the Seaglider SGX or Teledyne Slocum G3 glider. The extended energy bay, larger

498   buoyancy range, and thruster should make the operation of the coastal Slocum G3 with HydroC

499   sensors relatively easy and would allow for autonomous high-resolution water column

500   measurements of pCO_2 and pCH_4 in dynamic coastal environments. The integration of a HydroC

501   on a Slocum glider will require a custom-made wet-payload bay due to the size of this sensor.

502   For open ocean or deeper coastal regions, the integration with the Seaglider SGX, with 60%

503   higher energy capacity, would be effective and nearly identical to the work already done here.

504   The SG HydroC CH_4 was successfully integrated into the Seaglider as part of this project.

505   While tank experiments showed promising results, short field tests of the CH_4 Seaglider in

506   shallow water revealed low and patchy methane concentrations near the detection limit (not

507   shown). The CH_4 Seaglider requires further testing in environments with strong pCH_4 gradients

508   during longer and deeper dives (to allow for equilibration) to assess the accuracy of its

509   response time-corrected data in the field. The sensor's slow response time likely limits the glider

510   to providing qualitative rather than quantitative results. However, due to the scarcity of oceanic

511   CH_4 observations, deploying a CH_4 glider can help identify the location of methane sources and

512   guide the placement of in situ observations to conduct a more quantitative assessment of CH_4

513   fluxes and dynamics.

514   Ocean gliders are part of the Intergovernmental Oceanographic Commission (IOC-

515   UNESCO) Global Ocean Observing System (GOOS) through the OceanGliders program

516   (https://www.oceangliders.org/). Like other elements of the GOOS coordinated by OceanOPs of

517   the Observation Coordination Group (floats, buoys, moorings, ships, and tide gauges),

518   OceanGliders contributes to "Ocean Observation for Climate, Ocean Health and Real Time

519   Services". CO_2 gliders are perfectly suited to contribute data for understanding relevant

520   inorganic carbon processes in coastal shelf and boundary regions where mesoscale or sub-

521   mesoscale variability dominates. The current work can also serve as a first step to bring together

522   interested scientists and engineers to further develop and improve the capability of gliders to

523   measure high-quality data. OceanGliders supports this effort by promoting the formation of

524   volunteer international task teams, for which a task team could be requested for oceanographic

525   greenhouse gas research. By doing this, the visibility and availability of data will be improved as

526   well, since GOOS provides an interactive data platform for all its programs (https://www.ocean-

527   ops.org/board). An OceanGliders task team could also be linked with the GOOS-sponsored

528   Global Climate Observing System (GCOS: https://gcos.wmo.int/en/home) program through their

529   Ocean Observations Physics and Climate Panel (OOPC): "a scientific expert advisory group

530   charged with making recommendations for a sustained global ocean observing system for

531   climate."

532

533   **5. Concluding Thoughts**

534   Near real-time and high-resolution water column data that can be retrieved from gliders

535   outfitted with sensors measuring salinity, temperature, inorganic carbon system parameters,

536   oxygen, and pCH$_4$ are key to tackling a variety of today's climate change-related issues. These

537   datasets will become instrumental in advancing biogeochemical model forecasting and early

538   warning systems for extreme heat, acidity, and oxygen compound events that affect coastal

539   subsistence communities, commercial fisheries, and mariculture. Furthermore, using

540   biogeochemical gliders to monitor the environment of tagged organisms (e.g. crabs, fish) would

541   provide insight into the organism's position and behavior relative to important environmental

542   drivers across susceptible ecosystems. Such biogeochemical glider data will help bridge in situ

543   chemical and biological measurements, and environmental change to impacts on biology, and

544   thereby fill an important research gap (Widdicomb et al., 2023). Potentially large natural and

545   anthropogenic sources of CH_4 may become contributors to climate change, and if oxidized, to

546   ocean acidification (Garcia-Tigreros et al., 2021; Sparrow et al., 2018; Shakhova et al., 2010;

547   Rees et al., 2022). These CH_4 sources need to be properly assessed and quantified, and if

548   characterized as anthropogenic origin, emitters must be held accountable (Goodman et al., 2022).

549   Once the combined HydroC CH_4/CO_2 is available it will provide a new tool to co-measure pCH_4

550   and pCO_2 and give valuable insight into these processes and feedback mechanisms. Other

551   advancing fields, such as marine Carbon Dioxide Removal (mCDR) and monitoring,

552   verification, and reporting (MRV) thereof will also need detailed knowledge of the distribution

553   of CO_2 in the water column (National Academies of Sciences, Engineering, and Medicine.

554   2022).

555   The CO_2 Seaglider has been extensively tested and is ready to be used in open ocean

556   environments. An important next step will be to integrate the HydroC CO_2 and CH_4 sensors into

557   a glider platform that reliably functions in shallow, and freshwater-affected coastal areas, such as

558   the Gulf of Alaska, to be able to fill the large spatial and temporal data gap in these highly

559   dynamic areas.

560

561   **Data availability**

562   The CO_2 Seaglider data is publicly available (Hauri et al., 2022; 2023). The HydroC-

563   specific SIRMA code and CNF file are available on Github (Cyprus-Subsea, 2024a and 2024b).

564   More detailed information on the HydroC – glider integration and operation can be found in the

565   CO_2 Seaglider Standard Operating Procedures (Irving et al., 2024).

566

567   **Author contributions**

568   C.H. and A.M. developed the research ideas and the proposal that funded this work. C.H.

569   led the fieldwork and writing of this manuscript. B.I. led the preparation for fieldwork and glider

570   data processing and analysis. D.H. led glider piloting for all trials. D.H. and E.A. assisted with

571   data processing, sensor programming, mechanical integration, glider ballasting, deployment, and

572   recovery. N.K. and J.K. provided technical support for the HydroC sensors. All authors

573   contributed to the writing of this manuscript.

574

575   **Competing interests**

576   Authors Hayes and Abdi are employed by AOOI and CSCS (respectively) and their

577   objective is to support the ocean research community by providing innovative, cutting-edge

578   observing technological solutions. These include autonomous platforms and related services in

579   unique configurations. Through the support of the National Science Foundation and the National

580   Oceanographic Partnership Program, AOOI was able to jointly develop the CO_2 and CH_4 gliders

581   and prove and improve the scientific utility of this approach. Authors Kinski and Kemme are

582   employed by -4H-JENA engineering GmbH, the manufacturer of the HydroC CO_2 and CH_4

583   sensors. The objective of -4H-JENA engineering GmbH is to provide best possible accuracy of

584   dissolved gas measurements on any platform and at any environmental condition. Intensive

585   collaboration with scientists is essential for the development of these products.

586

Acknowledgments

Financial support

611 **References**

612 Aßmann, S., Frank, C., and Körtzinger, A.: Spectrophotometric high-precision seawater

613 pH determination for use in underway measuring systems, Ocean Sci., 7, 597–

614 607, https://doi.org/10.5194/os-7-597-2011, 2011.

615

616 Barnes, R. O. and Goldberg, E. D. Methane production and consumption in anoxic marine

617 sediments. Geology 4, 297–300, 1976.

618

619 Bittig, H. C., Körtzinger, A., Neill, C., van Ooijen, E., Plant, J. N., Hahn, J., Johnson, K. S.,

620 Yang, B., and Emerson, S. R.: Oxygen Optode Sensors: Principle, Characterization, Calibration,

621 and Application in the Ocean, Front. Mar. Sci., 4, https://doi.org/10.3389/fmars.2017.00429,

622 2018.

623

624 Bockmon, E. E. and Dickson, A. G.: A seawater filtration method suitable for total dissolved

625 inorganic carbon and pH analyses, Limnology and Oceanography Methods, 12(4), 191–195,

626 https://doi.org/10.4319/lom.2014.12.191, 2014.

627

628 Breitberg, D., Salisbury, J., Bernhard, J., Cai, W.-J., Dupont, S., Doney, S., Kroeker, K., Levin,

629 L., Long, W. C., Milke, L., Miller, S., Phelan, B., Passow, U., Seibel, B., Todgham, A., and

630 Tarrant, A.: And on Top of All That… Coping with Ocean Acidification in the Midst of Many

631 Stressors, Oceanography, 25, 48–61, https://doi.org/10.5670/oceanog.2015.31, 2015.

632

633 Breitburg, D., Levin, L. A., Oschlies, A., Grégoire, M., Chavez, F. P., Conley, D. J., Garçon, V.,

29

634   Gilbert, D., Gutiérrez, D., Isensee, K., Jacinto, G. S., Limburg, K. E., Montes, I., Naqvi, S. W.

635   A., Pitcher, G. C., Rabalais, N. N., Roman, M. R., Rose, K. A., Seibel, B. A., Telszewski, M.,

636   Yasuhara, M., and Zhang, J.: Declining oxygen in the global ocean and coastal waters, Science,

637   359, 46, https://doi.org/10.1126/science.aam7240, 2018.

638

639   Briggs, E. M., Martz, T. R., Talley, L. D., Mazloff, M. R., and Johnson, K. S.: Physical and

640   Biological Drivers of Biogeochemical Tracers Within the Seasonal Sea Ice Zone of the Southern

641   Ocean From Profiling Floats, J. Geophys. Res. Oceans, 123, 746–758,

642   https://doi.org/10.1002/2017JC012846, 2018.

643

644   Chavez, F. P., Sevadjian, J., Wahl, C., Friederich, J., and Friederich, G. E.: Measurements

645   of pCO$_2$ and pH from an autonomous surface vehicle in a coastal upwelling system, Deep Sea

646   Res. Part II Top. Stud. Oceanogr., 151, 137–146, https://doi.org/10.1016/j.dsr2.2017.01.001,

647   2018.

648

649   Claustre, H., Johnson, K. S., and Takeshita, Y.: Observing the Global Ocean

650   with Biogeochemical-Argo, Annu. Rev. Mar. Sci., 12, 23–48, https://doi.org/10.1146/annurev-

651   marine-010419-010956, 2020.

652

653   Clayton, T. D. and Byrne, R. H.: Spectrophotometric seawater pH measurements: total hydrogen

654   ion concentration scale calibration of m-cresol purple and at-sea results, Deep Sea Res. Part

655   Oceanogr. Res. Pap., 40(10), 2115–2129, 1993.

656

657   Cyprus-Subsea: Smart-Cable-HydroC, GitHub repository [code], https://github.com/Cyprus-

658   Subsea/Smart-Cable-HydroC (last access: 14 June 2024), 2024a.

659

660   Cyprus-Subsea: CO_2 and CH_4 CNF files, GitHub repository [code], https://github.com/Cyprus-

661   Subsea/Smart-Cable-HydroC/tree/main/docs (last access: 7 July 2024), 2024b.

662

663   DeGrandpre, M. D., Lai, C. Z., Timmermans, M. L., Krishfield, R. A., Proshutinsky, A.,

664   and Torres, D.: Inorganic Carbon and $p$$CO_2$ Variability During Ice Formation in the Beaufort

665   Gyre of the Canada Basin, J. Geophys. Res. Oceans, 124, 4017–4028,

666   https://doi.org/10.1029/2019JC015109, 2019.

667

668   Dickson, A. G.: Thermodynamics of the dissociation of boric acid in synthetic seawater

669   from 273.15 to 318.15 K, Deep Sea Res. Part Oceanogr. Res. Pap., 37, 755–

670   766, https://doi.org/10.1016/0198-0149(90)90004-F, 1990.

671

672   Dickson, A. G., Sabine, C. L., and Christian J.R.: Guide to Best Practices for Ocean

673   CO_2 Measurements, PICES Spec. Publ. 3, 191, 2007.

674

675   Dølven, K. O., Vierinen, J., Grilli, R., Triest, J., and Ferré, B.: Response time correction of slow-

676   response sensor data by deconvolution of the growth-law equation, Geosci. Instrum. Methods

677   Data Syst., 11, 293–306, https://doi.org/10.5194/gi-11-293-2022, 2022.

678

679   Doney, S. C., Fabry, V. J., Feely, R. A., and Kleypas, J. A.: Ocean Acidification: The Other

680 CO$_2$ Problem, Annu. Rev. Mar. Sci., 1, 169–192,

681 https://doi.org/10.1146/annurev.marine.010908.163834, 2009.

682

683 Du, M. et al. High resolution measurements of methane and carbon dioxide in surface waters

684 over a natural seep reveal dynamics of dissolved phase air–sea flux. Environ. Sci. Technol. 48,

685 10165–10173 (2014).

686

687 Fiedler, B., Fietzek, P., Vieira, N., Silva, P., Bittig, H. C., and Körtzinger, A.: In situ CO$_2$ and

688 O$_2$ measurements on a profiling float, J. Atmospheric Ocean. Technol., 30, 112–

689 126, https://doi.org/10.1175/JTECH-D-12-00043.1, 2013.

690

691 Fietzek, P., Fiedler, B., Steinhoff, T., and Körtzinger, A.: In situ quality assessment of a novel

692 underwater pCO$_2$ sensor based on membrane equilibration and NDIR spectrometry, J.

693 Atmospheric Ocean. Technol., 31, 181–196, https://doi.org/10.1175/JTECH-D-13-00083.1,

694 2014.

695

696 Garcia-Tigreros, F., Leonte, M., Ruppel, C. D., Ruiz-Angulo, A., Joung, D. J., Young, B.,

697 and Kessler, J. D.: Estimating the Impact of Seep Methane Oxidation on Ocean pH

698 and Dissolved Inorganic Radiocarbon Along the U.S. Mid-Atlantic Bight, J. Geophys. Res.

699 Biogeosciences, 126, e2019JG005621, https://doi.org/10.1029/2019JG005621, 2021.

700

701 Goodman, S., Davies, P., Maddox, M., and Durkee, J.: Arctic Methane – Situational Awareness,

702 Assessment and Policy Directions, Results of the June 23rd, 2022 Arctic Methane Workshop,

703   Summary Report, 2022.

704

705   Gruber, N., Clement, D., Carter, B. R., Feely, R. A., van Heuven, S., Hoppema, M., Ishii, M.,

706   Key, R. M., Kozyr, A., Lauvset, S. K., Lo Monaco, C., Mathis, J. T., Murata, A., Olsen, A.,

707   Perez, F. F., Sabine, C. L., Tanhua, T., and Wanninkhof, R.: The oceanic sink for anthropogenic

708   CO_2 from 1994 to 2007, Science, 363, 1193–1199,

709   https://doi.org/10.1126/science.aau5153, 2019.

710

711   Gruber, N., Boyd, P. W., Frölicher, T. L., and Vogt, M.: Biogeochemical extremes

712   and compound events in the ocean, Nature, 600, 395–407, https://doi.org/10.1038/s41586-021-

713   03981-7, 2021.

714

715   Hauri, C., McDonnell, A., Winsor, P., Irving, B., and Statscewich, H.: Development of

716   an Autonomous Carbon Glider to Monitor Sea-Air CO_2 Fluxes in the Chukchi Sea, Bureau of

717   Ocean Energy Management, 2018.

718

719   Hauri, C., Irving, B., Hayes, D., Abdi, E., Kemme, J., Kinski, N., McDonnell,

720   A.M.P.: CO_2 Seaglider trajectory file from Gulf of Alaska 2022.

721   SEANOE. https://doi.org/10.17882/100964, 2022.

722

723   Hauri, C., Irving, B., Hayes, D., Abdi, E., Kemme, J., Kinski, N., McDonnell,

724   A.M.P.: CO_2 Seaglider trajectory file from Gulf of Alaska 2023.

725   SEANOE. https://doi.org/10.17882/100965, 2023.

726

727 Hauri, C., Pagès, R., Hedstrom, K., Doney, S. C., Dupont, S., Ferriss, B., and Stuecker, M. F.:

728 More Than Marine Heatwaves: A New Regime of Heat, Acidity, and Low Oxygen Compound

729 Extreme Events in the Gulf of Alaska, AGU Adv., 5, e2023AV001039,

730 https://doi.org/10.1029/2023AV001039, 2024.

731

732 Hemming, M. P., Kaiser, J., Heywood, K. J., Bakker, D. C. E., Boutin, J., Shitashima, K., Lee,

733 G., Legge, O., and Onken, R.: Measuring pH variability using an experimental sensor on an

734 underwater glider, Ocean Sci., 13, 427–442, https://doi.org/10.5194/os-13-427-2017, 2017.

735

736 Irving, B., Hauri, C., Hayes, D., Abdi, E., Kinski., N.: Carbon Dioxide SOP, Version 1.0.0.

737 (GitHub Repository, Carbon Dioxide

738 SOP, https://britairving.github.io/Carbon_Dioxide_SOP/README.html (last access: 7 July,

739 2024).

740

741 Islam, F., DeGrandpre, M. D., Beatty, C. M., Timmermans, M.-L., Krishfield, R. A., Toole, J.

742 M., and Laney, S. R.: Sea surface CO_2 and O_2 dynamics in the partially ice-covered Arctic

743 Ocean, J. Geophys. Res. Oceans, 122, 1425–1438, https://doi.org/10.1002/2016JC012162, 2017.

744

745 Jiang, L.-Q., Feely, R. A., Wanninkhof, R., Greeley, D., Barbero, L., Alin, S., Carter, B. R.,

746 Pierrot, D., Featherstone, C., Hooper, J., Melrose, C., Monacci, N., Sharp, J. D., Shellito, S., Xu,

747 Y.-Y., Kozyr, A., Byrne, R. H., Cai, W.-J., Cross, J., Johnson, G. C., Hales, B., Langdon, C.,

748 Mathis, J., Salisbury, J., and Townsend, D. W.: Coastal Ocean Data Analysis Product in North

749 America (CODAP-NA) – an internally consistent data product for discrete inorganic carbon,

750 oxygen, and nutrients on the North American ocean margins, Earth Syst. Sci. Data, 13, 2777–

751 2799, https://doi.org/10.5194/essd-13-2777-2021, 2021.

752

753 Johnson, G. C. and Lyman, J. M.: Warming trends increasingly dominate global ocean,

754 Nat. Clim. Change, 10, 757–761, https://doi.org/10.1038/s41558-020-0822-0, 2020.

755

756 Kessler, J. Atlantic bubble bath. Nature Geosci 7, 625–

757 626, https://doi.org/10.1038/ngeo2238, 2014.

758

759 Kroeker, K. J., Kordas, R. L., and Harley, C. D. G.: Embracing interactions in

760 ocean acidification research: Confronting multiple stressor scenarios and context dependence,

761 Biol. Lett., 13, https://doi.org/10.1098/rsbl.2016.0802, 2017.

762

763 Laufkötter, C., Zscheischler, J., and Frölicher, T. L.: High-impact marine heatwaves attributable

764 to human-induced global warming, Science, 369, 1621–

765 1625, https://doi.org/10.1126/science.aba0690, 2020.

766

767 Lauvset, S. K., Lange, N., Tanhua, T., Bittig, H. C., Olsen, A., Kozyr, A., Alin, S., Álvarez, M.,

768 Azetsu-Scott, K., Barbero, L., Becker, S., Brown, P. J., Carter, B. R., da Cunha, L. C., Feely, R.

769 A., Hoppema, M., Humphreys, M. P., Ishii, M., Jeansson, E., Jiang, L.-Q., Jones, S. D., Lo

770 Monaco, C., Murata, A., Müller, J. D., Pérez, F. F., Pfeil, B., Schirnick, C., Steinfeldt,

771 R., Suzuki, T., Tilbrook, B., Ulfsbo, A., Velo, A., Woosley, R. J., and Key, R. M.:

772   GLODAPv2.2022: the latest version of the global interior ocean biogeochemical data product,

773   Earth Syst. Sci. Data, 14, 5543–5572, https://doi.org/10.5194/essd-14-5543-2022, 2022.

774

775   Lee, K., Kim, T.-W., Byrne, R. H., Millero, F. J., Feely, R. A., and Liu, Y.-M.: The universal

776   ratio of boron to chlorinity for the North Pacific and North Atlantic oceans, Geochim.

777   Cosmochim. Acta, 74, 1801–1811, https://doi.org/10.1016/j.gca.2009.12.027, 2010.

778

779   Leonte, M., Kessler, J. D., Kellermann, M. Y., Arrington. E. C., Valentine, D. L., Sylva, S.

780   P.: Rapid rates of aerobic methane oxidation at the feather edge of gas hydrate stability in the

781   waters of Hudson Canyon, US Atlantic Margin. Geochim. Cosmochim. Acta 204, 375–

782   387, https://doi.org/10.1016/j.gca.2017.01.009, 2017.

783

784   Lueker, T. J., Dickson, A. G., and Keeling, C. D.: Ocean pCO$_2$ calculated from dissolved

785   inorganic carbon , alkalinity , and equations for K 1 and K 2 : validation based on laboratory

786   measurements of CO$_2$ in gas and seawater at equilibrium, Mar. Chem., 70, 105–

787   119, https://doi.org/10.1016/S0304-4203(00)00022-0, 2000.

788

789   Manley, J. and Willcox, S.: The Wave Glider: A persistent platform for ocean science,

790   in: OCEANS'10 IEEE SYDNEY, OCEANS'10 IEEE SYDNEY, 1–

791   5, https://doi.org/10.1109/OCEANSSYD.2010.5603614, 2010.

792

793   McGinnis, D. F., Greinert, J., Artemov, Y., Beaubien, S. E. & Wüest, A. Fate of rising methane

794   bubbles in stratified waters: How much methane reaches the atmosphere? J. Geophys.

795   Res. 111, https://doi.org/10.1029/2005jc003183, 2006.

796

797   Metzl, N., Fin, J., Lo Monaco, C., Mignon, C., Alliouane, S., Antoine, D., Bourdin, G., Boutin,

798   J., Bozec, Y., Conan, P., Coppola, L., Diaz, F., Douville, E., Durrieu de Madron, X., Gattuso, J.-

799   P., Gazeau, F., Golbol, M., Lansard, B., Lefèvre, D., Lefèvre, N., Lombard, F., Louanchi,

800   F., Merlivat, L., Olivier, L., Petrenko, A., Petton, S., Pujo-Pay, M., Rabouille, C., Reverdin, G.,

801   Ridame, C., Tribollet, A., Vellucci, V., Wagener, T., and Wimart-Rousseau, C.: A synthesis of

802   ocean total alkalinity and dissolved inorganic carbon measurements from 1993 to 2022: the

803   SNAPO-CO2-v1 dataset, Earth Syst. Sci. Data, 16, 89–120, https://doi.org/10.5194/essd-16-89-

804   2024, 2024.

805

806   Meurer, W. P., Blum, J., and Shipman, G.: Volumetric Mapping of Methane Concentrations at

807   the Bush Hill Hydrocarbon Seep, Gulf of Mexico, Front. Earth Sci.,

808   9, https://doi.org/10.3389/feart.2021.604930, 2021.

809

810   Monacci, N.M.; Bott, R.; Cross, J.N.; Dougherty, S.; Maenner, S.; Musielewicz, S.; Osborne, J.;

811   Sutton, A. (2023). High-resolution ocean and atmosphere pCO$_2$ time-series measurements from

812   mooring GAKOA_149W_60N. High-resolution ocean and atmosphere pCO$_2$ time-series

813   measurements from mooring GAKOA_149W_60N in the Gulf of Alaska (NCEI Accession

814   0116714). NOAA National Centers for Environmental

815   Information. Dataset. https://doi.org/10.3334/cdiac/otg.tsm_gakoa_149w_60n

816

817   Manley, J. and Willcox, S.: The Wave Glider: A persistent platform for ocean science, in:

818   OCEANS'10 IEEE SYDNEY, OCEANS'10 IEEE SYDNEY, 1–

819   5, https://doi.org/10.1109/OCEANSSYD.2010.5603614, 2010.

820

821   Miloshevich, L. M., Paukkunen, A., Vömel, H., and Oltmans, S. J.: Development and

822   Validation of a Time-Lag Correction for Vaisala Radiosonde Humidity Measurements,

823   J. Atmospheric Ocean. Technol., 21, 1305–1327, https://doi.org/10.1175/1520-

824   0426(2004)021<1305:DAVOAT>2.0.CO;2, 2004.

825

826   Myhre, G., Shindell, D., Bréon, F.-M., Collins, W., Fuglestvedt, J., Huang, J., Koch, D.,

827   Lamarque, J.-F., Lee, D., Mendoza, B., Nakajima, T., Robock, A., Stephens, G., Takemura, T.,

828   and Zhang, H.: Anthropogenic and Natural Radiative Forcing, in: Climate Change 2013: The

829   Physical Science Basis, Contribution of Working Group I to the Fifth Assessment Report of

830   the Intergovernmental Panel on Climate Change, edited by: Stocker, T. F., Qin, D., Plattner, G.-

831   K., Tignor, M., Allen, S. K., Boschung, J., Nauels, A., Xia, Y., Bex, V., and Midgley, P.

832   M., Cambridge University Press, Cambridge, UK, New York, NY, USA, 2013.

833

834   National Academies of Sciences, Engineering, and Medicine: A Research Strategy for Ocean-

835   based Carbon Dioxide Removal and Sequestration. Washington, DC: The National

836   Academies Press. https://doi.org/10.17226/26278, 2022.

837

838   Newton, J. A., Feely, R. A., Jewett, E. B., Williamson, P., and Mathis, J.: Global

839   ocean acidification observing network: requirements and governance plan, GOA-

840   ON, Washington, 61 pp., 2015.

841

842 Nickford, S., Palter, J. B., Donohue, K., Fassbender, A. J., Gray, A. R., Long, J., Sutton, A. J.,

843 Bates, N. R., and Takeshita, Y.: Autonomous Wintertime Observations of Air-Sea Exchange in

844 the Gulf Stream Reveal a Perfect Storm for Ocean CO_2 Uptake, Geophys. Res. Lett., 49,

845 e2021GL096805, https://doi.org/10.1029/2021GL096805, 2022.

846

847 von Oppeln-Bronikowski, N., de Young, B., Atamanchuk, D., and Wallace, D.: Glider-based

848 observations of CO_2 in the Labrador Sea, Ocean Sci., 17, 1–16, https://doi.org/10.5194/os-17-1-

849 2021, 2021.

850

851 OceanGliders Oxygen SOP: https://nora.nerc.ac.uk/id/eprint/533559/, last access: 24

852 January 2024.

853

854 Orr, J. C., Epitalon, J. M., Dickson, A. G., and Gattuso, J. P.: Routine uncertainty propagation

855 for the marine carbon dioxide system, Mar. Chem., 207, 84–

856 107, https://doi.org/10.1016/j.marchem.2018.10.006, 2018.

857

858 Perez, F. F. and Fraga, F.: Association constant of fluoride and hydrogen ions in seawater, Mar.

859 Chem., 21, 161–168, https://doi.org/10.1016/0304-4203(87)90036-3, 1987.

860

861 Pinnau, I., and Toy, L. G.: Gas and vapor transport properties of amorphous perfluorinated

862 copolymer membranes based on 2,2-bistrifluoromethyl-4,5-difluoro-1,3-

863 dioxole/tetrafluoroethylene, Journal of Membrane Science, 109 (1), 125-

864   133, https://doi.org/10.1016/0376-7388(95)00193-X, 1996.

865

866   Possenti, L., Humphreys, M. P., Bakker, D. C. E., Cobas-García, M., Fernand, L., Lee, G. A.,

867   Pallottino, F., Loucaides, S., Mowlem, M. C., and Kaiser, J.: Air-Sea Gas Fluxes and

868   Remineralization From a Novel Combination of pH and O_2 Sensors on a Glider, Front. Mar. Sci.,

869   8, 1–19, https://doi.org/10.3389/fmars.2021.696772, 2021.

870

871   Reeburgh, W. Oceanic methane biogeochemistry. Am. Chem. Soc. 107, 486–513, 2007.

872

873   Sarmiento, J. L. and Gruber, N.: Ocean Biogeochemical Dynamics, Princeton University Press,

874   Princeton, NJ, 526 pp., ISBN 9780691017075, 2006.

875

876   Qi, D., Ouyang, Z., Chen, L., Wu, Y., Lei, R., Chen, B., Feely, R. A., Anderson, L. G., Zhong,

877   W., Lin, H., Polukhin, A., Zhang, Y., Zhang, Y., Bi, H., Lin, X., Luo, Y., Zhuang, Y., He, J.,

878   Chen, J., and Cai, W. J.: Climate change drives rapid decadal acidification in the Arctic Ocean

879   from 1994 to 2020, Science, 377, 1544–1550, https://doi.org/10.1126/science.abo0383, 2022.

880

881   Rees, A. P., Bange, H. W., Arévalo-Martínez, D. L., Artioli, Y., Ashby, D. M., Brown, I.,

882   Campen, H. I., Clark, D. R., Kitidis, V., Lessin, G., Tarran, G. A., and Turley, C.: Nitrous oxide

883   and methane in a changing Arctic Ocean, Ambio, 51, 398–410, https://doi.org/10.1007/s13280-

884   021-01633-8, 2022.

885

886   Saba, G. K., Wright-Fairbanks, E., Chen, B., Cai, W. J., Barnard, A. H., Jones, C. P., Branham,

887   C. W., Wang, K., and Miles, T.: The Development and Validation of a Profiling Glider Deep

888   ISFET-Based pH Sensor for High Resolution Observations of Coastal and Ocean Acidification,

889   Front. Mar. Sci., 6, 1–17, https://doi.org/10.3389/fmars.2019.00664, 2019.

890

891   Sabine, C. L. and Tanhua, T.: Estimation of anthropogenic CO_2 inventories in the ocean., Annu.

892   Rev. Mar. Sci., 2, 175–98, https://doi.org/10.1146/annurev-marine-120308-080947, 2010.

893

894   Sabine, C. L., Feely, R. A., Gruber, N., Key, R. M., Lee, K., Bullister, J. L., Wanninkhof, R.,

895   Wong, C. S., Wallace, D. W. R., Tilbrook, B., Millero, F. J., Peng, T.-H., Kozyr, A., Ono, T.,

896   and Rios, A. F.: The oceanic sink for anthropogenic CO_2, Science, 305, 367–

897   71, https://doi.org/10.1126/science.1097403, 2004.

898

899   Sejr, M. K., Krause-Jensen, D., Rysgaard, S., Sørensen, L. L., Christensen, P. B., and Glud, R.

900   N.: Air-sea flux of CO_2 in arctic coastal waters influenced by glacial melt water and sea ice,

901   Tellus B, 63, 815–822, https://doi.org/10.1111/j.1600-0889.2011.00540.x, 2011.

902

903   Sharp, J. D., Pierrot, D., Humphreys, M. P., Epitalon, J.-M., Orr, J. C., Lewis, E. R., and

904   Wallace, D. W. R.: CO2SYSv3 for MATLAB, , https://doi.org/10.5281/zenodo.7552554, 2023.

905

906   Shakhova, N., Semiletov, I., Salyuk, A., Yusupov, V., Kosmach, D., and Gustafsson, Ö.:

907   Extensive Methane Venting to the Atmosphere from Sediments of the East Siberian Arctic Shelf,

908   Science, 327, 1246–1250, https://doi.org/10.1126/science.1182221, 2010.

909

910   Skarke, A., Ruppel, C., Kodis, M., Brothers, D. and Lobecker, E. Widespread methane leakage

911   from the sea floor on the northern US Atlantic margin. Nat. Geosci. 7, 657 (2014).

912

913   Sparrow, K. J., Kessler, J. D., Southon, J. R., Garcia-Tigreros, F., Schreiner, K. M., Ruppel, C.

914   D., Miller, J. B., Lehman, S. J., and Xu, X.: Limited contribution of ancient methane to surface

915   waters of the U.S. Beaufort Sea shelf, Sci. Adv., 4, eaao4842,

916   https://doi.org/10.1126/sciadv.aao4842, 2018.

917

918   Sulpis, O., Lauvset, S. K., and Hagens, M.: Current estimates of K and K appear inconsistent

919   with measured CO_2 system parameters in cold oceanic regions, Ocean Sci., 16, 847–

920   862, https://doi.org/10.5194/os-16-847-2020, 2020.

921

922   Takeshita, Y., Jones, B. D., Johnson, K. S., Chavez, F. P., Rudnick, D. L., Blum, M., Conner, K.,

923   Jensen, S., Long, J. S., Maughan, T., Mertz, K. L., Sherman, J. T., and Warren, J. K.: Accurate

924   pH and O_2 Measurements from Spray Underwater Gliders, J. Atmospheric Ocean. Technol., 38,

925   181–195, https://doi.org/10.1175/JTECH-D-20-0095.1, 2021.

926

927   Thompson, T., Saba, G. K., Wright-Fairbanks, E., Barnard, A. H., and Branham, C. W.:

928   Best Practices for Sea-Bird Scientific deep ISFET-based pH sensor integrated into a Slocum

929   Webb Glider, in: OCEANS 2021: San Diego – Porto, OCEANS 2021: San Diego – Porto, 1–8,

930   https://doi.org/10.23919/OCEANS44145.2021.9706067, 2021.

931

932   Vergara-Jara, M. J., DeGrandpre, M. D., Torres, R., Beatty, C. M., Cuevas, L. A., Alarcón, E.,

933   and Iriarte, J. L.: Seasonal changes in carbonate saturation state and air-sea CO_2 fluxes during an

934   annual cycle in a stratified-temperate fjord (Reloncaví Fjord, Chilean Patagonia), J. Geophys.

935   Res. Biogeosciences, 124, 2851–2865, https://doi.org/10.1029/2019jg005028, 2019.

936

937   Widdicombe, S., Isensee, K., Artioli, Y., Gaitán-Espitia, J. D., Hauri, C., Newton, J. A., et

938   al.: Unifying biological field observations to detect and compare ocean acidification impacts

939   across marine species and ecosystems: What to monitor and why. Ocean Science, 19(1), 101–

940   119. https://doi.org/10.5194/os-19-101-2023, 2023.

941

942   Woosley, R. J. and Millero, F. J.: Freshening of the western Arctic negates anthropogenic carbon

943   uptake potential, Limnol. Oceanogr., https://doi.org/10.1002/lno.11421, 2020.

944

945   Wright-Fairbanks, E. K., Miles, T. N., Cai, W.-J., Chen, B., and Saba, G. K.:

946   Autonomous Observation of Seasonal Carbonate Chemistry Dynamics in the Mid-Atlantic

947   Bight, J. Geophys. Res. Oceans, 125,

948   e2020JC016505, https://doi.org/10.1029/2020JC016505, 2020.

949

950

951

952

Tables

Table 1. Tank experiment. Evaluation of SG HydroC CO_2 and SG HydroC CH_4 sensors

compared to reference discrete pCO_2^{disc} and pCH_4^{disc}. Units of pCO_2 and $pCH4$ are µatm except

when shown as percent difference in parenthesis (Equation 1). Columns with subscripts sn422

and sn0718 indicate data from sensors HydroC CO2T-0422-001 and HydroC CO2T-0718-001,

respectively. Superscript RTC indicates response time corrected values following Dølven et al.

(2022). pCO_2^{disc} and pCH_4^{disc} values are the average of triplicate bottles and are shown in Figure

6.

961

Triplicate Date Time (UTC)	$pCO_2^{disc} \pm$ uc (µatm)	$pCO_{2,sn422}^{RTC}$- pCO_2^{disc}	$pCO_{2,sn0718}^{RTC}$ - pCO_2^{disc}	$pCH_4^{disc} \pm u$ (µatm)	pCH_4^{RTC} - pCH_4^{disc}
5/2/2022 3:25	298.7 ± 10.2	-0.9 (-0.3%)	-	-	-
5/2/2022 7:32	227.1 ± 7.8	4.3 (1.9%)	2.4 (1.1%)	-	-
5/2/2022 11:27	223.3 ± 7.7	0.7 (0.3%)	-2.6 (-1.2%)	-	-
5/2/2022 15:30	227.8 ± 7.9	-1.1 (-0.5%)	-3.3 (-1.4%)	-	-
5/2/2022 00:11	-	-	-	25.4 ± 2.1	4.0 (15.8 %)
5/2/2022 12:06	-	-	-	7.3 ± 1.3	0.5 (6.6 %)

962

963

964 **Table 2. Profiling experiment.** Evaluation of SG HydroC CO_2 sensor compared to reference

965 discrete pCO_2^{disc}. Units of pCO_2 are µatm except when shown as percent difference in

966 parenthesis (Eq. 1). pCO_2 with subscripts sn422 indicate data from the HydroC installed on the

967 rosette (HydroC CO2T-0422-001). The superscript RTC indicates response time corrected values

968 following Dølven et al. (2022).

Discrete Date Time (UTC)	Discrete Depth (m)	$pCO_2^{disc} \pm uc$ (µatm)	$pCO_{2,sn422}^{RTC} - pCO_2^{disc}$
5/3/2022 21:21	2.5	214.5 ± 7.5	5.4 (2.5%)
5/3/2022 21:39	19.9	246.8 ± 8.5	1.6 (0.6 %)
5/3/2022 22:33	9.6	244.4 ± 8.5	-3.3 (-1.4 %)
5/3/2022 22:34	9.7	234.7 ± 8.1	8.2 (3.5 %)

969

970

971 **Table 3. Seaglider HydroC evaluation with a nearby cast.** Evaluation of Seaglider integrated

972 and rosette mounted SG HydroC CO2 sensors compared to pCO_2^{disc} collected from a nearby cast.

973 Units of pCO_2 are µatm except when shown as percent difference in parenthesis (Eq. 1) and

974 differences between $pCO_{2,Seaglider}^{RTC}$ were calculated with the average (upcast and downcast

975 combined) 1-meter binned data. The superscript RTC indicates response time corrected values

976 following Dølven et al. (2022), and subscripts Rosette and Seaglider indicate the SG HydroC

977 CO_2 sensor mounted on the rosette (SG HydroC CO2T-0422-001) and integrated into the

978 Seaglider (SG HydroC CO2T-0718-001), respectively. Time delay (HH:MM) and spatial

979 distance (km) columns represent the distance between $pCO_{2,Seaglider}^{RTC}$ measured at the discrete

980 depth and the discrete date time. The asterisk (*) indicates the comparison with $pCO_{2,Rosette}^{RTC}$

981 taken as nearest in time before sensor zeroing (Figure S1).

Discrete Date Time (UTC)	Discrete Depth (m)	$pCO_2^{disc} \pm$ uc (µatm)	$pCO_{2,Rosette}^{RTC}$ - pCO_2^{disc}	Delay (HH:MM)	Distance (km)	$pCO_{2,Seaglider}^{RTC}$ - pCO_2^{disc}
5/7/2022 18:06	71.8	349.7 ± 7.8	-5.7 (-1.6 %)	02:47	0.4	10.2 (2.9 %)
5/7/2022 18:24	57.1	313.8 ± 6.7	12.1 (3.9 %)	03:05	0.6	8.3 (2.7 %)
5/7/2022 18:42	19.8	285.3 ± 6.1	0.8 (0.3 %)	03:23	0.8	8.6 (3.0 %)
5/7/2022 19:00	1.6	233.4 ± 5.0	-2.3 (-1.0 %)*	03:41	0.9	12.0 (5.1 %)

982

983
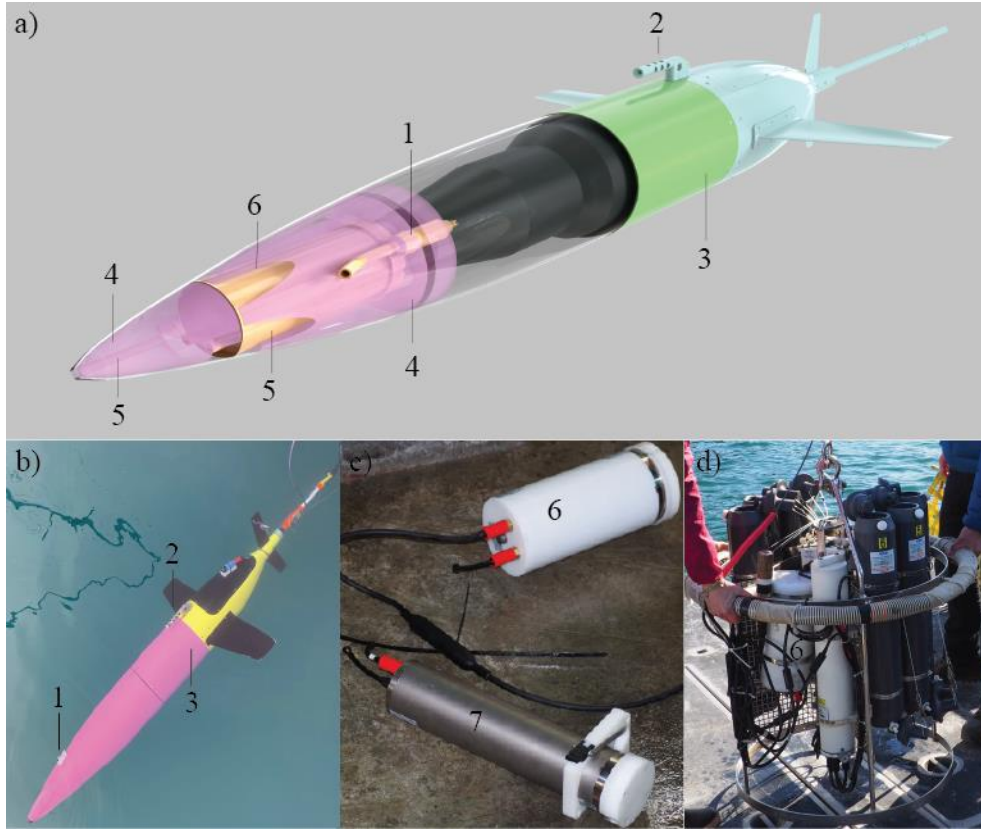
Figures

986   **Figure 1. CO₂ Seaglider.** CO$_2$ Seaglider a) schematic rendering and b) picture in Resurrection

987   Bay, Seward, Alaska, during a checkout dive on 6 February 2023, before beginning the first

988   winter mission collecting high resolution pCO$_2$ data. Highlighted are 1) SeaBird 5M pump, 2)

989   conductivity and temperature sail, 3) extension, 4) syntactic foam, 5) water flow channels, and 6)

990   SG HydroC CO$_2$ in a titanium housing, enabling pCO$_2$ observations down to 1000 m. c) Picture

991   of new SG HydroC CO$_2$ in a polyoxymethylene housing (6, rated to 300 m depth) and original

992   CONTROS HydroC^{TM} CO$_2$ (7). d) Picture of rosette set up for profiling experiment.

993

Figure 2. SG HydroC CO₂ sensor mounting designs. a) Titanium SG HydroC CO₂ (rated to

1000m) in a custom syntactic foam coat and b) polyoxymethylene SG HydroC CO₂ (rated to

300m) with brackets.

997
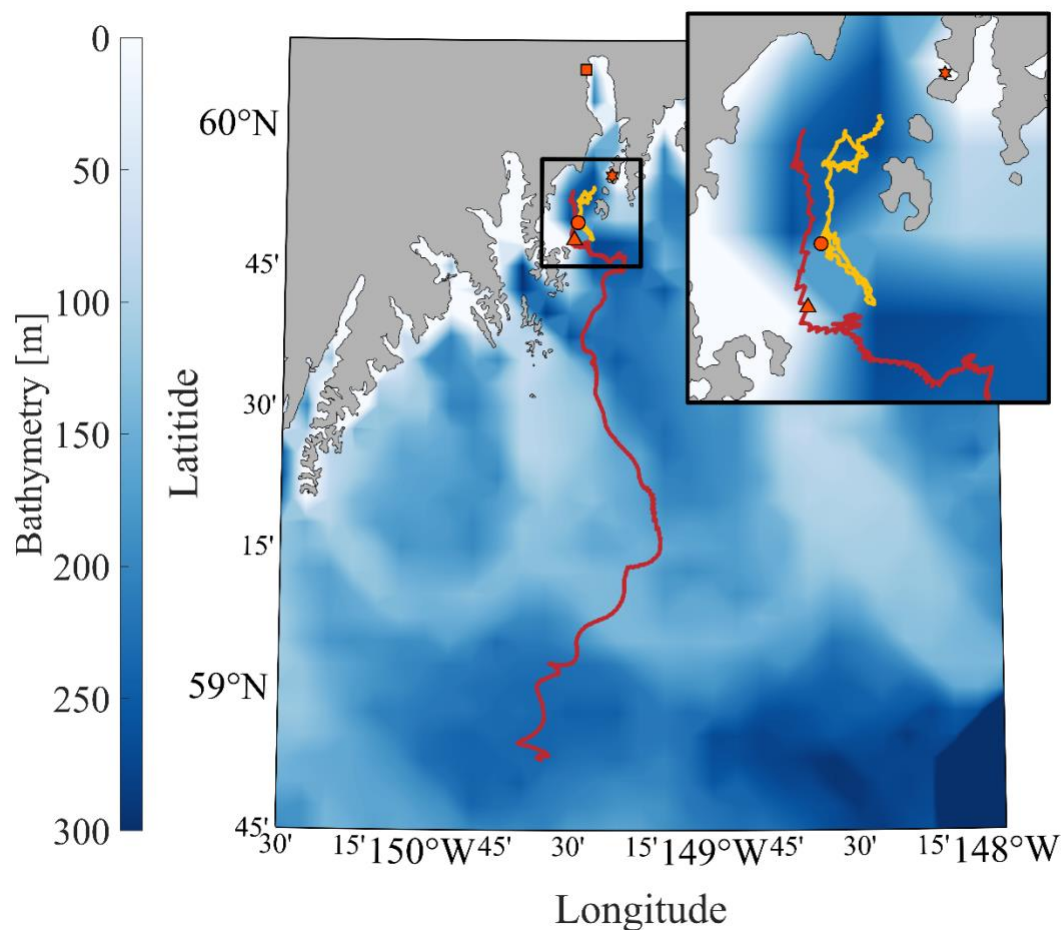
Figure 3. Map of CO₂ Seaglider study area. The bathymetry of the Gulf of Alaska is shown in

color with zoomed in section of the head of Resurrection Bay (outlined black square and inset

map). Tracks of the CO₂ Seaglider from the 4 – 7 May 2022 and 8 – 21 February 2023 missions

are shown in yellow and red, respectively. Orange markers outlined in black show the location of

the Alutiiq Pride Marine Institute (square), National Oceanic and Atmospheric Administration's

Gulf of Alaska Ocean Acidification mooring (star), 7 May CTD cast (circle), and last location

where pCO₂ was collected during the February 2023 mission (triangle).

1005

1006   moving median filter applied to the RTC data. Black diamonds with red filling show discrete

1007 $p\mathrm{CH_4}^{\mathrm{disc}}$ and all discrete values of $p\mathrm{CO_2}^{\mathrm{disc}}$ and $p\mathrm{CH_4}^{\mathrm{disc}}$ are the average of triplicate bottles.
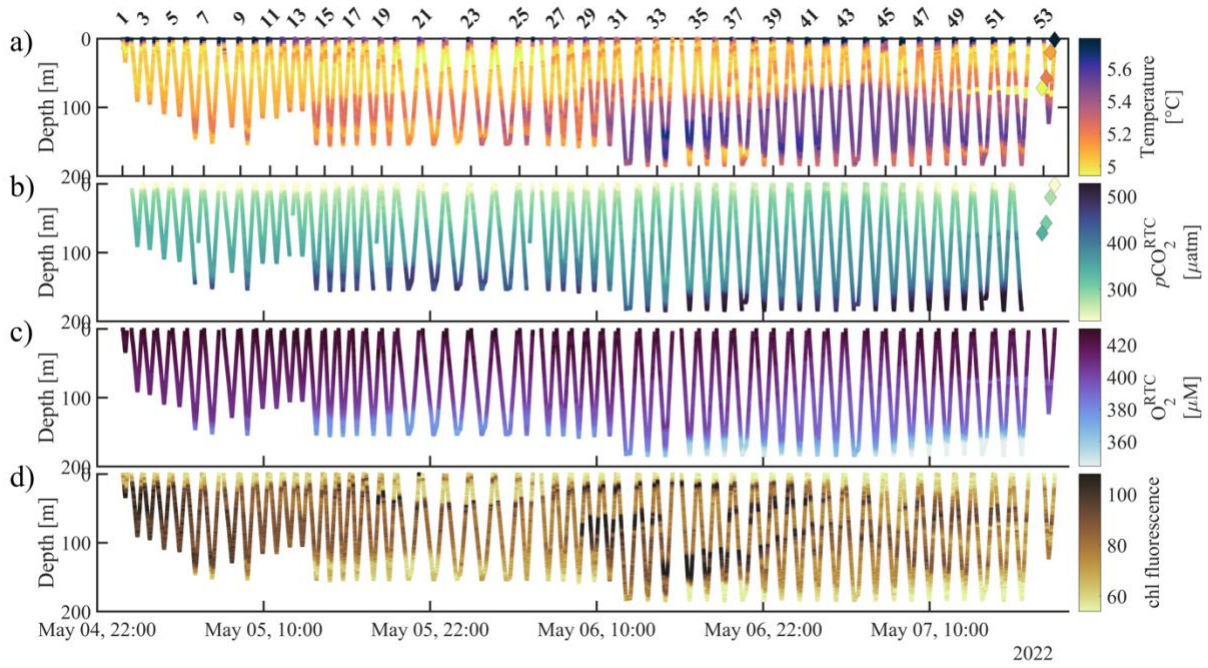
1008

1009   **Figure 4. CO₂ Seaglider data from the 4 – 7 May 2022 mission in Resurrection Bay,**

1010   **Seward, Alaska.** Depth profiles of a) Temperature [°C], b) RTC $p\mathrm{CO_2}$ [µatm] c) RTC $\mathrm{O_2}$ [µM],

1011   and d) raw chlorophyll fluorescence. The diamonds show discrete values that were taken during

1012   a CTD cast (Table 3).
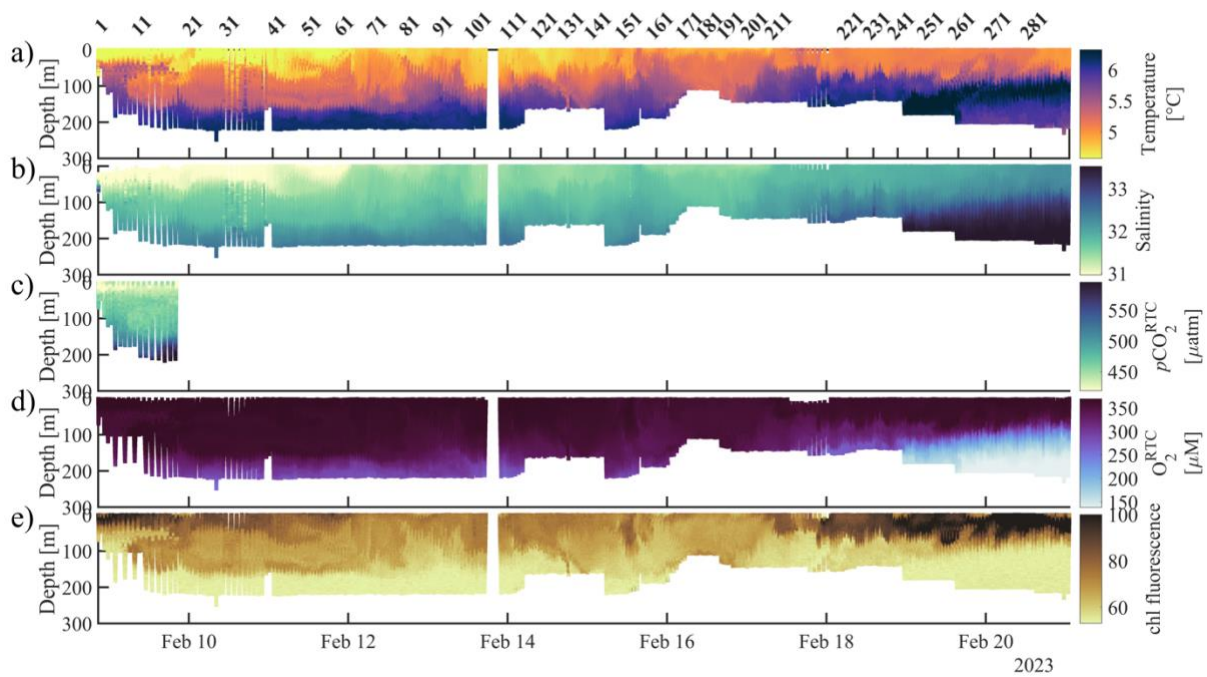
1013

Figure 5. CO₂ Seaglider data collected during the 8 – 21 February 2023 winter mission.

Shown are a) temperature (°C), b) salinity, c) response time corrected pCO₂ (pCO₂^{RTC}, μatm), d)

response time corrected oxygen (O₂^{RTC}, μM), and e) raw chlorophyll fluorescence (chl

fluorescence) as time/dive number vs. pressure.

1018
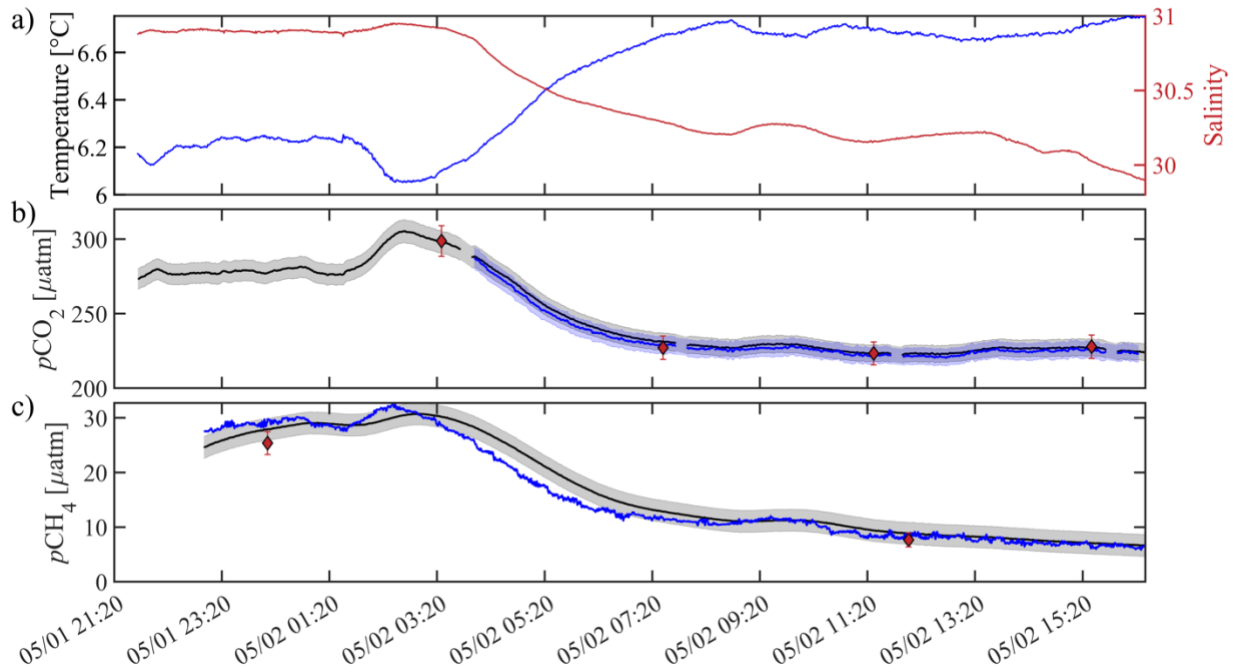
1019

Figure 6. Sensor validation during a tank experiment at the Alutiiq Pride Marine Institute

on 1 – 2 May 2022. a) temperature (blue line) and salinity (red line) from a recently calibrated

Sea-Bird Scientific SBE37. b) black (blue) lines show pCO_2 in µatm from HydroC CO2T-0422-

001 (HydroC CO2T-0718-001) with the shaded gray (blue) areas showing a relative uncertainty

of 2.5% (weather quality goal; Newton et al., 2015). Black circles with red filling show discrete

pCO_2^{disc} with error bars showing the combined standard uncertainty from *errors.m* (Orr et al.,

2018). HydroC pCO_2 data are shown at 1 minute resolution with a 2-minute moving median

filter applied and have not been corrected for response time, but differences were negligible (<

0.1 µatm). c) Black line shows pCH_4 in µatm from HydroC CH4T-0422-001 with the shaded

gray bar showing an uncertainty of 2 µatm. The blue line is the response time corrected signal

with a response time of 43 minutes following Dølven et al., (2022). HydroC pCH_4 data are

1031   shown at 1 minute resolution with a 2-minute moving median filter applied to the raw data and a

1032   10-minute
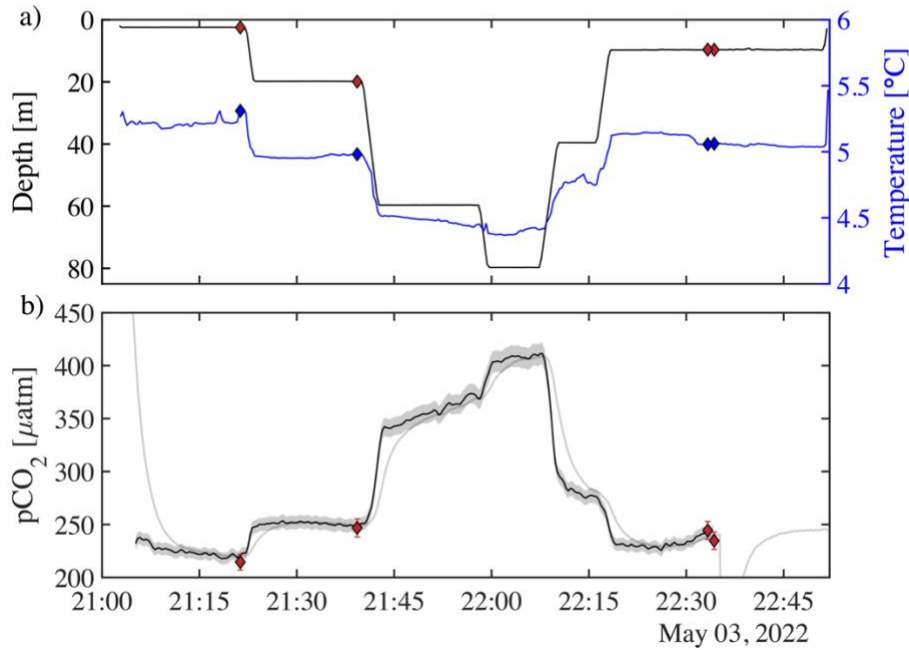
1033

1034   **Figure 7. Profiling experiments from 3 May 2022 with HydroC CO2T-0422-001 sensor**

1035   **mounted on the rosette.** a) Pressure vs time on the left (black) axis with diamonds showing

1036   rosette CTD values of pressure (red filled diamond), and temperature vs time on the right (blue)

1037   axis and temperature (blue filled diamond) at the time of the bottle fire. b) $p\mathrm{CO}_2$ measured by

1038   the rosette mounted SG HydroC CO_2 sensor as raw (gray line) and response time corrected

1039   signal (thick black line; $p\mathrm{CO}_{2,\mathrm{sn422}}^{\mathrm{RTC}}$ in Table 2) with shaded relative uncertainty of 2.5%

1040   (weather goal; Newton et al., 2015). $p\mathrm{CO}_2^{\mathrm{disc}}$ shown as red diamonds with vertical red error bars

1041   showing combined standard uncertainty (Orr et al., 2018). Table 2 shows differences between

1042   discrete $p\mathrm{CO}_2^{\mathrm{disc}}$ and $p\mathrm{CO}_{2,\mathrm{sn422}}^{\mathrm{RTC}}$. The SG HydroC CO_2 sensor started a zeroing interval at

1043   22:35 on 3 May 2022, so $p\text{CO}_{2,\text{sn422}}{}^{\text{RTC}}$ is not shown after that time but signal recovery can be

1044   seen in the uncorrected signal (gray line).

1045

1046
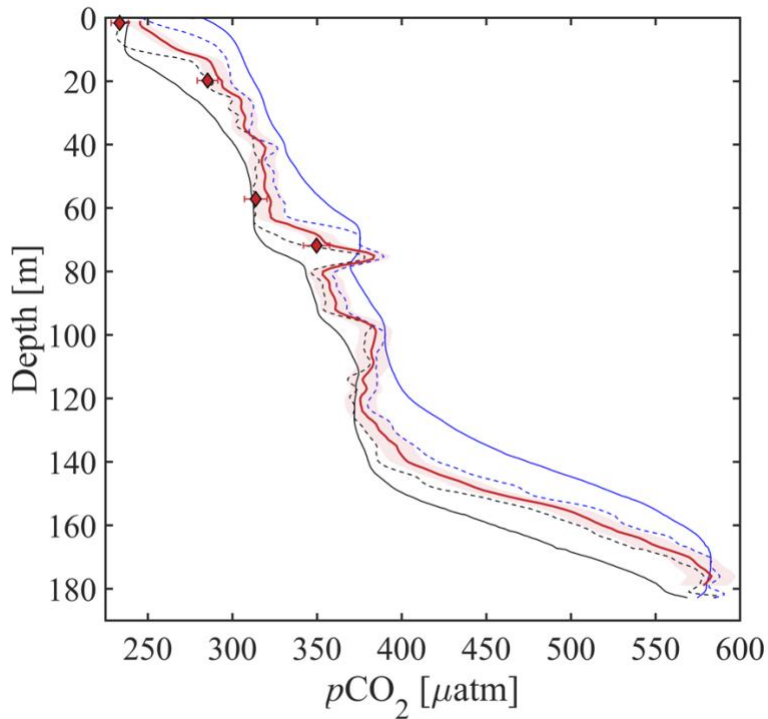
1047

1048   **Figure 8. CO$_2$ Seaglider data from a single dive during the 4 – 7 May 2022 mission in**

1049   **Resurrection Bay, Seward, Alaska.** Depth profile of pCO$_2$ in µatm showing the original

1050   resolution smoothed pCO$_2$ used in the RT correction (downcast = solid black, upcast = solid

1051   blue), RTC pCO$_2$ following Dølven et al. (2022) (dashed black line = downcast, dashed blue line

1052   = upcast), and 1-meter binned RTC profile (thick red line) with red shading showing the relative

1053   uncertainty of 2.5 %. Discrete pCO$_2^{disc}$ shown as red diamonds with horizontal red error bars

1054   showing combined standard uncertainty (Orr et al., 2018). Differences between pCO$_2^{disc}$ and

1055 pCO$_{2,Seaglider}^{RTC}$ are shown in Table 3.

1056
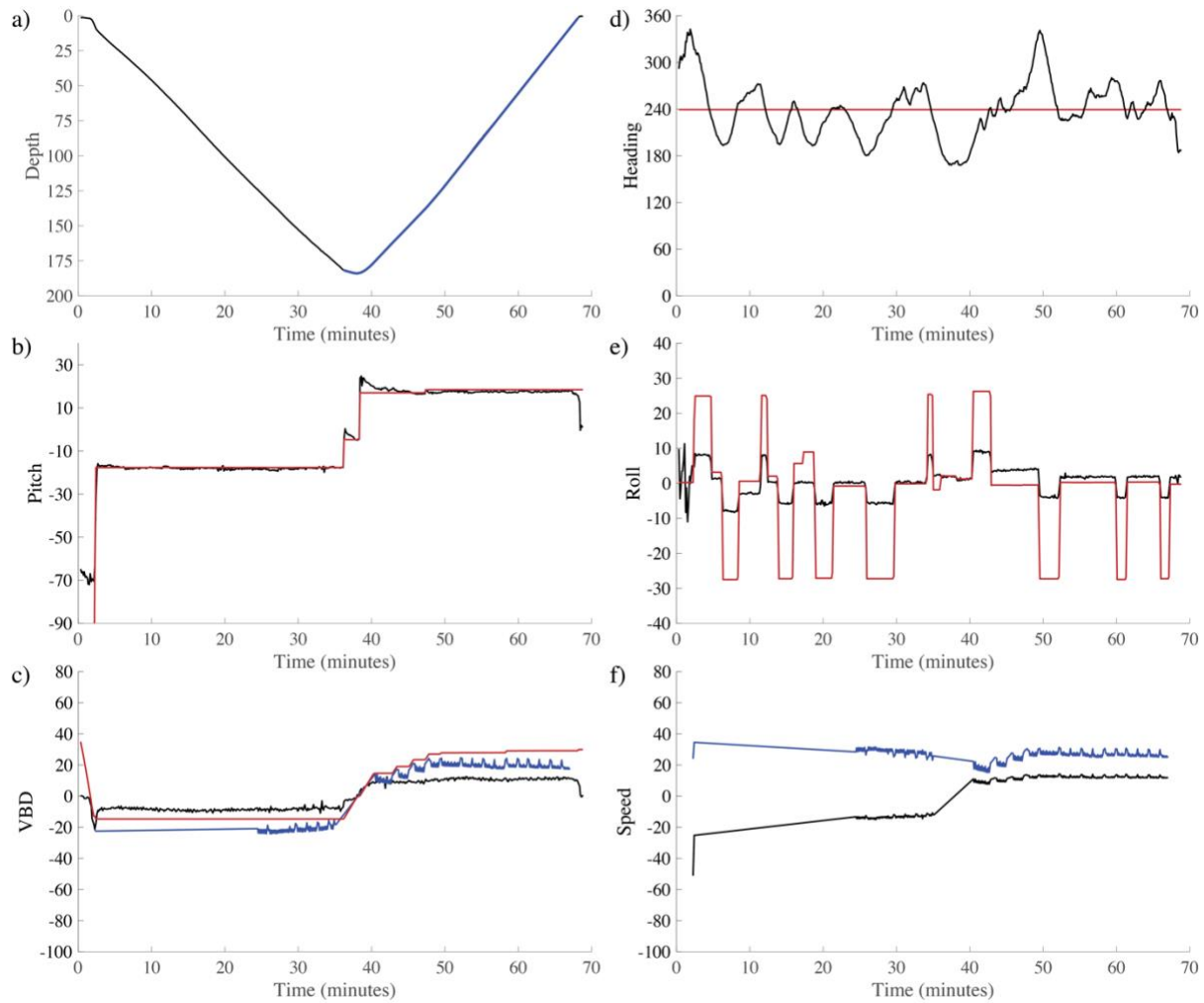
1057

Figure 9. Dive details for the 300 m rated CO$_2$ Seaglider (dive# 51). a) Depth (black line,

meters), b) pitch (black line, degrees) with pitch control (red line, mm of battery shift), c)

Change in displacement of Variable Buoyancy Drive (VBD) (red line, units of 10 cc), vertical

velocity from pressure measurements (black line, cm/s), and buoyancy (blue line, units of 10 g),

d) heading in (desired red line, measured black line, degrees), e) roll (battery roll position red

line, glider measured roll black line, degrees), and f) vertical speed (calculated from buoyancy

and pitch, black line, cm/s) and horizontal speed (calculated from buoyancy and pitch, blue line,

cm/s).
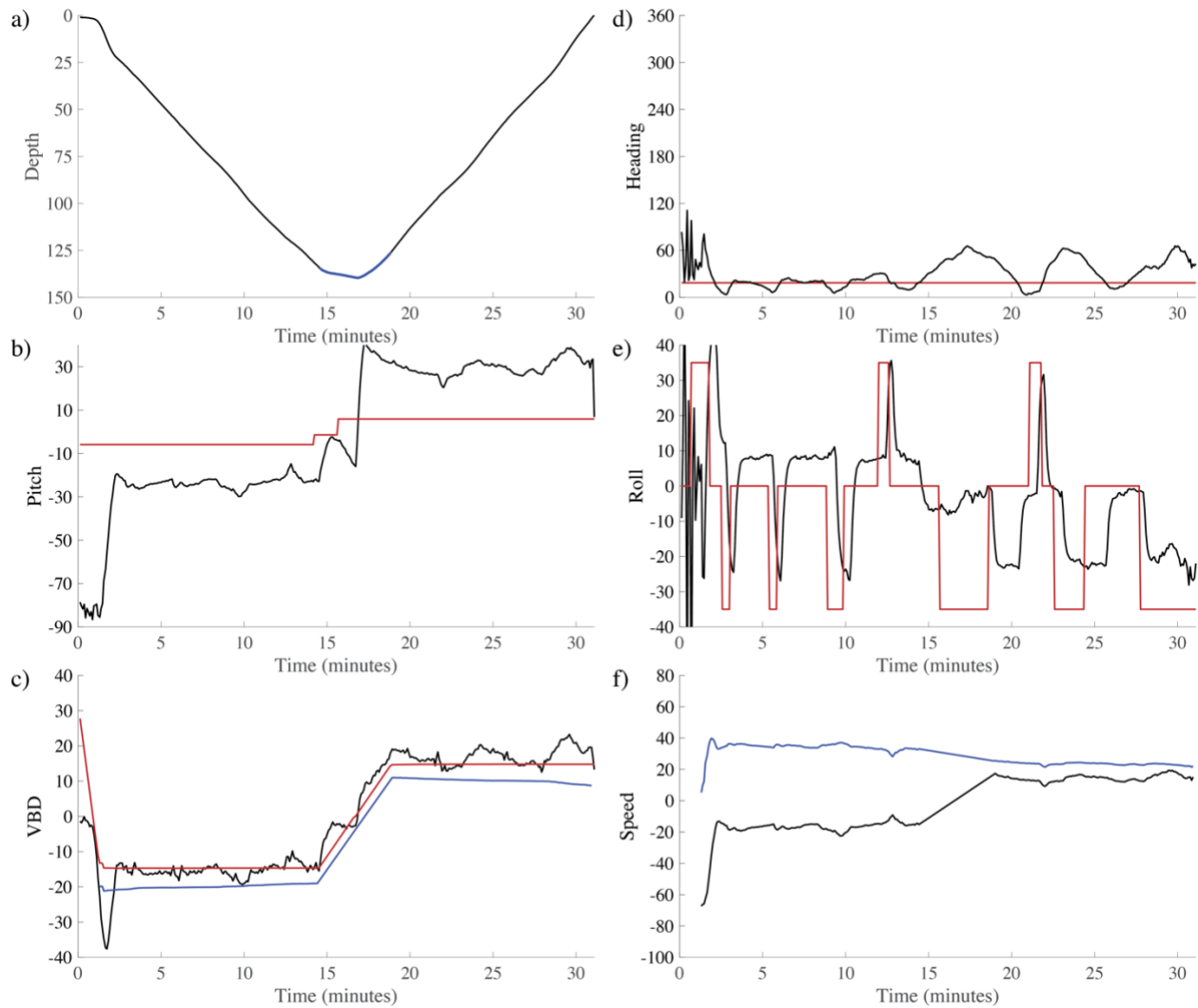
1066

Figure 10. Dive details for the 1000 m rated CO_2 Seaglider (dive# 203). a) Depth (black line,

meters), b) pitch (black line, degrees) with pitch control (red line, mm of battery shift), c)

Change in displacement of Variable Buoyancy Drive (VBD) (red line, units of 10 cc), vertical

velocity from pressure measurements (black line, cm/s), and buoyancy (blue line, units of 10 g),

d) Heading (desired heading red line, measured heading black line, degrees) e) roll (battery roll

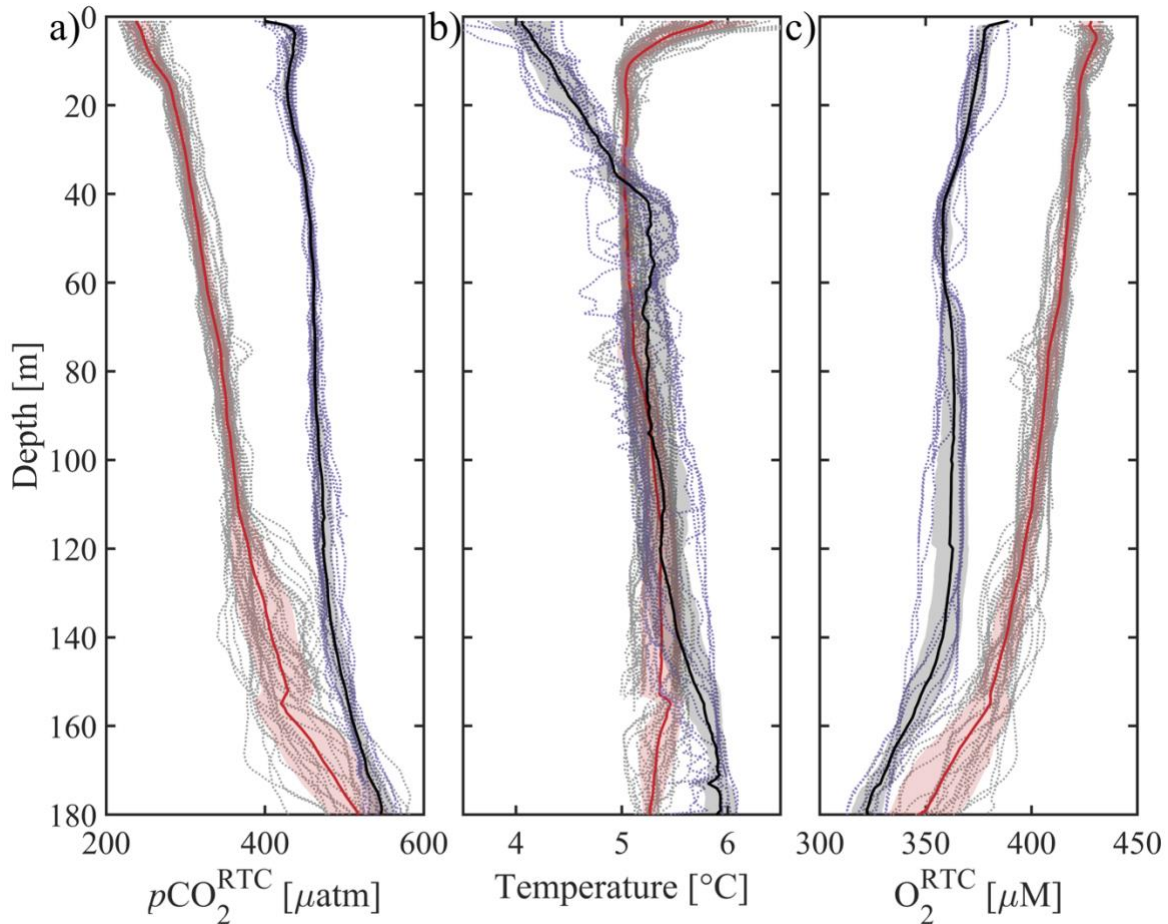position red line, glider measured roll black line, degrees), and f) vertical speed (calculated from

buoyancy and pitch, black line, cm/s) and horizontal speed in cm/s (calculated from buoyancy

and pitch, blue line, cm/s).

Figure 11. Averaged CO₂ Seaglider profiles from the 4 – 7 May 2022 and 8 – 21 February 2023 missions in Resurrection Bay, Seward, Alaska. Depth profiles of all 1-meter binned dives (dotted gray), average 1-meter binned dive from May 2022 mission (red thick line, dive#1-51, 00:01 5 May to 16:37 7 May, 2022) and February 2023 mission (black thick line, dive#1-17, 20:50 8 February to 19:54 9 February, 2023) with shading showing the standard deviation of the

1084   values in each bin added and subtracted from the average. a) Response time corrected pCO_2

1085   ($pCO_2{}^{RTC}$, µatm), b) temperature [°C], and c) response time corrected oxygen ($O_2{}^{RTC}$, µM).

1086

1087

1088
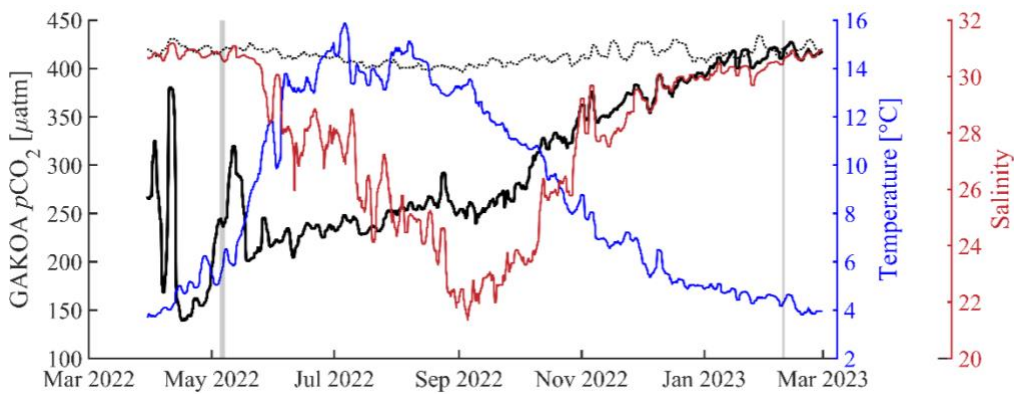
1089

1090   **Figure 12. National Oceanic Atmospheric Administration's Gulf of Alaska ocean**

1091   **acidification surface time-series from March 2022 - 2023.** Left axis sea surface (dotted black

1092   line) and air (black line, 4 meter above sea level) pCO_2 [uatm] and right axes sea surface

1093   temperature (blue, °C) and sea surface salinity (red). All data shown as 3 day running mean.

1094   Vertical shaded gray areas highlight the CO_2 Seaglider missions in May 2022 and February

1095   2023. The mooring is located at 59.911 °N, -149.35 °W (Monacci et al., 2023).

1096

1097

1098

1099